Hierarchical Control for Vehicle Platoons With Cut-in/Cut-Out Maneuvers via Distributed Model Predictive Control

Wenbo Li, Shuyou Yu, *Member, IEEE*, Yangyang Feng, Haoran Qi, and Hong Chen, *Fellow, IEEE*

***Abstract*—In this paper, a hierarchical control scheme, including a decision-making layer and a control layer, is proposed for vehicle platoons executing vehicle-following, cut-in, and cut-out maneuvers. Based on a finite-state machine, the decision-making layer is designed to ensure collision avoidance for vehicle platoons. In the control layer, a distributed model predictive control strategy is employed in the outer-loop to generate a reference sequence, where a linear parameter-varying kinematic model is established to account for the coupling of the vehicle platoon. Incremental constraints are designed to ensure bumpless transfer control during phase switching. By selecting the sum of local cost functions as a Lyapunov candidate, the asymptotic consensus of the vehicle platoon is proven. Furthermore, considering the coupled longitudinal and lateral dynamics of vehicles, in the inner-loop, a nonlinear model predictive control strategy is proposed to track the reference sequence. The effectiveness of the hierarchical control scheme is validated through co-simulation using MATLAB and TruckSim.**

***Index Terms*—Hierarchical control, vehicle platoon, cut-in and cut-out maneuver, model predictive control.**

Nomenclature

v_x	Longitudinal velocity.
v_y	Lateral velocity.
γ	Yaw rate.
φ	Heading angle.
I_z	Yaw moment of inertia.
m	Vehicle mass.
F_{yf}	Lateral force of the front tire.
F_{yr}	Lateral force of the rear tire.
l_f	Distance from the center of gravity to the front axle.
l_r	Distance from the center of gravity to the rear axle.
α_f	Sideslip angle of the front tire.
α_r	Sideslip angle of the rear tire.
F_x	Desired longitudinal force.
δ_f	Front wheel steering angle.
h	Prediction horizon of the outer-loop.
τ_1	Sampling period of the outer-loop.
$\tilde{h}$	Prediction horizon of the inner-loop.
τ_2	Sampling period of the inner-loop.
p_x	Longitudinal displacement.
p_y	Lateral displacement.

Received 13 October 2024; revised 19 May 2025, 22 October 2025, and 9 January 2026; accepted 22 February 2026. Date of publication 19 March 2026; date of current version 2 June 2026. This work was supported in part by the National Natural Science Foundation of China under Grant 62473167 and in part by the Natural Science Foundation of Jilin Province under Grant 20240402079GH. The Associate Editor for this article was B. F. Ciuffo. *(Corresponding author: Shuyou Yu.)*

Wenbo Li, Shuyou Yu, Yangyang Feng, and Haoran Qi are with the National Key Laboratory of Automotive Chassis Integration and Bionics, Changchun 130025, China, and also with the Department of Control Science and Engineering, Jilin University, Changchun 130025, China (e-mail: liwb21@mails.jlu.edu.cn; shuyou@jlu.edu.cn; yyfeng19@mails.jlu.edu.cn; hrqi22@mails.jlu.edu.cn).

Hong Chen is with the College of Electronics and Information Engineering, Tongji University, Shanghai 200092, China, and also with the Department of Control Science and Engineering, Jilin University, Changchun 130025, China (e-mail: chenh@jlu.edu.cn).

Digital Object Identifier 10.1109/TITS.2026.3668357

I. Introduction

Vehicle platoons are rapidly developing in intelligent transportation systems, which have benefits for improving safety and traffic efficiency, and reducing fuel consumption [1], [2]. As presented in [3], a review analyzes the impacts of vehicle platooning on traffic systems.

The vehicle platoon consists of vehicle-following, cut-in, and cut-out maneuvers, as shown in Fig. 1. An essential objective of the vehicle platoon is to maintain a desired inter-vehicle spacing with dynamic cut-in or cut-out vehicles.

A. Literature Review

Considering only the vehicle-following maneuver of vehicle platoons, some studies have been developed. In general, vehicle platoons consist of vehicle models, communication topologies, inter-vehicle spacing policies, and controllers [4]. Controllers can be categorized into centralized and distributed [5]. However, centralized control methods cannot guarantee driving safety due to high packet-drop rates and high computational load [6]. Distributed control methods, which use only information from neighboring vehicles, can collaboratively manage vehicle platoons. With a predecessor-following communication topology and a symmetric bidirectional communication topology, a distributed proportional-integral-derivative (PID) controller is proposed in [7], in which consensus of vehicle platoons is established. Furthermore, it concludes that the convergence rate of the states of vehicles in the platoon with a predecessor-following topology is faster than that of the symmetric bidirectional topology. In [8], a distributed backstepping controller is proposed to ensure string stability

TABLE I
CUT-IN/CUT-OUT MANEUVER LITERATURE

Decision-making Layer	Single-vehicle	[21]–[23]
	Multi-vehicle	[24], [25], [26], [27], [28], [29], [30], [31], [32], [33], [34], [35], [36], [37], [38], [39], [40], [41], [42], [43], [44]
Manipulation Layer	Longitudinal Control	[24], [25], [26], [27], [31], [32], [34], [35], [36], [37], [39], [40]
	Longitudinal and Lateral Control	[28], [29], [30], [42], [44]
Performance	Asymptotic consensus	[24], [26], [27], [28], [29], [34], [42], [44]
	Collision avoidance	[24], [26], [27], [28], [29], [30], [31], [32], [33], [34], [35], [36], [37], [38], [39], [42], [43]

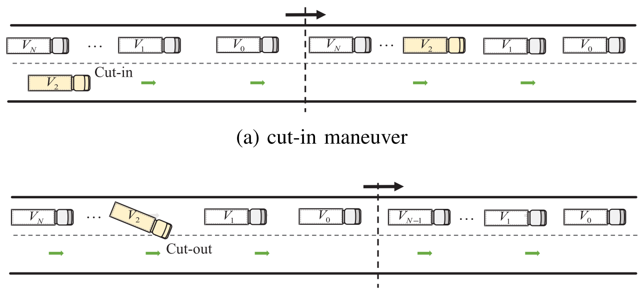

(a) cut-in maneuver

(b) cut-out maneuver

Fig. 1. Vehicle platoons with cut-in/cut-out maneuvers.

of the vehicle platoon. Asymptotic consensus is emphasized in vehicle platoons, i.e., the state of the following vehicles converges to that of the leading vehicle. In [9], a distributed PID controller is proposed to guarantee asymptotic consensus of vehicle platoons under fixed or switching communication topologies. Considering vehicle uncertainties, a distributed sliding mode controller and a distributed adaptive triple-step nonlinear controller are proposed to ensure asymptotic consensus of vehicle platoons in [10] and [11], respectively. However, it is pointed out that controllers designed by ignoring the nonlinear dynamics and constraints of vehicles may cause instability and unsafety in vehicle platoons [12].

Therefore, distributed model predictive control (DMPC) has been extensively developed for the vehicle-following maneuver of vehicle platoons, due to its advantages in effectively handling constraints and nonlinear dynamics of vehicles [13]. In [14], a review of the application of DMPC to vehicle platoons is presented, focusing on ensuring longitudinal asymptotic consensus and string stability. Considering collision avoidance constraints, a DMPC method is designed for heterogeneous vehicle platoons in [4], where a cost function is designed to penalize errors between predicted and assumed trajectories. Additionally, a terminal equality constraint is designed to ensure asymptotic consensus of vehicle platoons. Considering nonlinear longitudinal vehicle dynamics, a DMPC method is proposed in [15], which guarantees asymptotic consensus and string stability of vehicle platoons. Furthermore, DMPC based on the Koopman operator is designed in [16] to deal with nonlinear vehicle dynamics. For the vehicle-following maneuver on curved roads, DMPC is proposed for vehicle platoons to ensure asymptotic consensus in [17] and [18], where a coupled longitudinal and lateral vehicle dynamic model is adopted. However, the above research has only focused on the vehicle-following maneuver of vehicle platoons.

Cut-in and cut-out maneuvers of vehicle platoons have gained significant attention in merging and splitting scenarios [19]. A review of the research on vehicle platoons, considering not only the vehicle-following maneuver but also the cut-in and cut-out maneuvers, is presented in [20]. Here, some representative studies are presented in Table I and organized according to a hierarchical framework: a decision-making layer and a manipulation layer. The decision-making layer determines maneuvers for each vehicle. In the manipulation layer, vehicle controllers are designed to execute the maneuvers, which translate the high-level decisions into precise actions of the vehicles, such as throttling, braking, and steering.

The decision-making layer can be categorized into single-vehicle methods and multi-vehicle methods. Single-vehicle methods focus solely on making decisions for the cut-in or cut-out vehicle, ignoring the cooperative control among vehicles within the platoon [21], [22], [23]. However, such methods cannot guarantee the asymptotic consensus of vehicle platoons.

For multi-vehicle methods, the decision-making layer makes decisions for all vehicles. Considering only the cut-in maneuver, longitudinal control methods are proposed in the manipulation layers in [24], [25], [26], and [27]. Considering longitudinal and lateral control of vehicles, a distributed PID controller is developed for the cut-in maneuver in [28] and [29], where asymptotic consensus and collision avoidance are guaranteed. Considering the vehicle-following, cut-in, and cut-out maneuver, reinforcement learning-based decision-making layers are designed to make decisions for each vehicle in [30], [31], [32], and [33]. However, it may result in collisions between vehicles, due to the limitations in handling high-dimensional data and the risk of overfitting. Furthermore, receding horizon optimization-based decision-making layers are developed in [34], [35], [36], and [37]. A hierarchical control scheme is proposed in [34], where an optimization problem is formulated in the decision-making layer to calculate the global optimal sequence of vehicles, and a longitudinal sliding mode controller is developed in the manipulation layer. In [35], the A^* algorithm is adopted to determine the optimal sequence of vehicles in the decision-making layer. Then, a longitudinal trajectory planner and a tracking controller are designed in manipulation layer. Considering driving comfort and traffic efficiency, an optimization problem is formulated to determine the optimal cut-in position in the decision-making layer, and a longitudinal distributed PID controller is adopted in the manipulation layer [36]. In [37], taking into account fuel consumption, driving comfort, and traffic efficiency for the cut-in maneuver, an optimization problem is presented. However, the above studies based on the receding horizon optimization are computationally complex and ignore the lateral control of vehicles. In [38], a global motion planning framework for vehicle platoons is proposed based on a kinematic model, which accounts for optimal lane-change timing and motion energy for each vehicle. However, considering the nonlinear dynamics, the computational complexity increases significantly. Additionally, asymptotic consensus is not guaranteed within this framework.

Rule-based decision-making layers are designed using finite-state machines (FSMs), in which the cooperative control process of vehicle platoons is divided into a finite number of phases to simplify controller design. Some studies design decision-making layers based on FSMs while ignoring longitudinal or lateral vehicle control [39], [40], [41]. When only the cut-in maneuver is considered, an FSM that includes vehicle-following and cut-in phases is proposed as the decision-making layer [39], while a longitudinal DMPC is designed in the manipulation layer. In [40], two FSMs are proposed for the cut-in and cut-out maneuvers, respectively, while longitudinal and lateral vehicle control are not discussed. In [41], an FSM is proposed not only for the cut-in and cut-out maneuvers but also for autonomous emergency braking, and vehicle control is not developed. Furthermore, an FSM is designed for the cut-in maneuver of vehicle platoons in the decision-making layer, while a DMPC based on a vehicle kinematic model is developed for longitudinal and lateral control in the manipulation layer [42]. In [43], a hierarchical FSM framework is proposed to standardize the description of multiple maneuvers in vehicle platoons. In [44], a hierarchical control scheme is developed, in which an FSM incorporating following, merging, splitting, and lane-changing maneuvers is proposed, and a nonsingular terminal sliding-mode controller is designed to guarantee consensus. However, bumpless transfer control for phase switching in the FSM is not addressed. In [45], an excellent hybrid MPC framework is proposed based on the double-integrator vehicle model for the cooperative longitudinal control problem of accommodating simultaneous multi-vehicle cut-ins into a vehicle platoon, where different optimization problems are designed for the vehicle-following phase, spacing-preparation phase, and restoration phase, respectively. Notably, it not only ensures the feasibility and stability of the hybrid system during switching between lane-changing and vehicle-following, but also derives a lower bound on the lane-change time window via an MPC-based mixed-integer nonlinear programming optimizer. Moreover, the proposed MPC-based mixed-integer nonlinear programming optimizer ensures collision avoidance by optimizing lane-change timing and spacing. However, neglecting nonlinear vehicle dynamics introduces modeling errors, which may degrade the control performance of truck platooning systems.

B. Contributions and Organization

In this paper, a hierarchical control scheme comprising a decision-making layer and a control layer is proposed for vehicle-following, cut-in, and cut-out maneuvers of vehicle platoons. The main contributions of this paper are as follows:

First, existing DMPC approaches, including the longitudinal controller and the coupled controller, typically adopt terminal equality constraints to guarantee asymptotic consensus. However, obtaining the exact optimal solution for an optimization problem with equality constraints is difficult. This paper relaxes the strict terminal equality constraint to a terminal inequality constraint and demonstrates that asymptotic consensus still holds.

Second, existing FSM-based approaches typically switch the control law simultaneously with the driving phase, which may destroy the vehicle driving stability. To address this issue, an incremental control input constraint is introduced to ensure bumpless transfer control of vehicles during phase transitions. Additionally, it has been observed that calculating the terminal ingredients considering not only the incremental constraint but also both state and input constraints is still a challenge. To overcome this, a PLDI-based method for calculating the terminal ingredients of vehicle platoons is proposed.

Last, considering the complex models of the vehicle platoon, i.e., the coupled longitudinal and lateral vehicle dynamics and kinematics, it is challenging to design a cooperative control method that ensures driving safety and asymptotic consensus. A hierarchical control method that not only handles these complex models but also facilitates real-world implementation is proposed.

The subsequent sections of this paper are structured as follows. Section II presents the problem setup. Section III introduces the decision-making layer. Section IV designs the control layer. Section V demonstrates the effectiveness of the proposed scheme through co-simulation. Finally, Section VI concludes this paper.

C. Notations

Let $\mathbb{N}$, $\mathbb{Z}^+$, and $\mathbb{R}$ denote the sets of non-negative integers, positive integers, and real numbers, respectively. For any $a, b \in \mathbb{Z}^+$, $\mathbb{Z}^+_{[a,b]}$ represents the set $\left\{z \in \mathbb{Z}^+ \,|a \le z \le b\right\}$. For a vector $x \in \mathbb{R}^n$, $n \in \mathbb{Z}^+$, the symbol $\|x\|$ denotes its Euclidean norm, and $\|x\|_Q = \sqrt{x^{\mathrm{T}} Q x}$, where $Q \in \mathbb{R}^{n\times n}$ is positive semi-definite and the superscript T denotes its transpose. Furthermore, x^{max} and x^{min} represent the maximum and minimum elements of x, respectively. The symbol $\Delta x(k) = x(k) - x(k-1)$, where k is the time instant. For a matrix W, the inequality $W \ge 0$ indicates that W is positive semi-definite. Given matrices x_i, $i = 1, \ldots, n, n \in \mathbb{Z}^+$, $diag(x_1, \ldots, x_n)$ is a diagonal matrix with diagonal elements x_1 to x_n. $\mathbf{0}$ denotes a zero matrix of appropriate dimensions. $I_n \in \mathbb{R}^{n\times n}, n \in \mathbb{Z}^+$ is an n-dimensional identity matrix. The symbol $*$ signifies the transpose of a matrix block located symmetrically within the matrix. Within the framework of MPC, the term $t|k$ refers to the t-th prediction time instant, starting from the current time instant k.

II. Problem Setup

The vehicle-following, cut-in, and cut-out maneuvers of vehicle platoons are considered in this paper. A vehicle platoon consists of a leading vehicle (indexed by V_0), and N following vehicles (indexed from V_1 to V_N). In Fig. 1a, vehicle V_2 cuts into the vehicle platoon. In Fig. 1b, vehicle V_2 cuts out of the vehicle platoon. Then, a new platoon is formed, where all vehicles execute the vehicle-following maneuver. Note that vehicle V_0 is human-driven, and the cut-in or cut-out maneuvers are generally executed on a straight road.

A. Communication Topologies

Communication topologies include the predecessor-following, predecessor-leader-following, and two-predecessor-following types. The communication topology can be described by a directed graph $\mathbb{G} = \{\mathbb{V}, \mathbb{E}\}$, where $\mathbb{V} = \{1, \ldots, N\}$ is the set of following vehicles and $\mathbb{E} \subseteq \mathbb{V} \times \mathbb{V}$ is the set of edges representing communication links [46]. The communication matrix of the vehicle platoon is defined as $\mathcal{A} = [a_{i,j}] \in \mathbb{R}^{N \times N}$, where each entry $a_{i,j}$ is given by

$$\begin{cases} a_{i,j} = 1 & \text{if } \{i, j\} \in \mathbb{E} \\ a_{i,j} = 0 & \text{if } \{i, j\} \notin \mathbb{E} \end{cases} \tag{1}$$

Here, $(i, j) \in \mathbb{E}$ indicates that vehicle V_j sends information to vehicle V_i. In this paper, the predecessor-following communication topology is adopted.

B. Coupled Longitudinal and Lateral Vehicle Dynamics

A three-degree-of-freedom vehicle model, including longitudinal, lateral, and yaw motions, is presented as follows:

$$\dot{v}_{x,i} = v_{y,i}\gamma_i + \frac{F_{x,i}}{m}, \tag{2a}$$

$$\dot{v}_{y,i} = -v_{x,i}\gamma_i + \frac{F_{yf,i} + F_{yr,i}}{m}, \tag{2b}$$

$$\dot{\gamma}_i = \frac{l_f F_{yf,i} - l_r F_{yr,i}}{I_z}. \tag{2c}$$

In (2b) and (2c), lateral forces of the tires are described using the Magic Formula as follows:

$$\begin{aligned} F_{yf,i} = -D_{yf} \sin \big(C_{yf} \arctan \big(B_{yf}\alpha_{f,i} \\ - E_{yf} \left(B_{yf}\alpha_{f,i} - \arctan \left(B_{yf}\alpha_{f,i} \right) \right) \big) \big), \end{aligned} \tag{3}$$

and

$$\begin{aligned} F_{yr,i} = -D_{yr} \sin \big(C_{yr} \arctan \big(B_{yr}\alpha_{r,i} \\ - E_{yr} \left(B_{yr}\alpha_{r,i} - \arctan \left(B_{yr}\alpha_{r,i} \right) \right) \big) \big), \end{aligned} \tag{4}$$

where B_{yf}, C_{yf}, D_{yf}, and E_{yf} are constant coefficients of the front tire; B_{yr}, C_{yr}, D_{yr}, and E_{yr} are the constant coefficients of the rear tire.

In (3) and (4), the sideslip angles of the tires are defined as

$$\alpha_{f,i} = \delta_{f,i} - \frac{v_{y,i} + l_f\gamma_i}{v_{x,i}}, \tag{5a}$$

$$\alpha_{r,i} = \frac{l_r\gamma_i - v_{y,i}}{v_{x,i}}. \tag{5b}$$

Then, discrete-time nonlinear dynamics of the vehicles is described as follows:

$$\hat{x}_i(k+1) = f\left(\hat{x}_i(k), \hat{u}_i(k)\right), \tag{6}$$

where $\hat{x}_i = \left[v_{x,i}, v_{y,i}, \gamma_i\right]^{\mathrm{T}}$ is the state and $\hat{u}_i = \left[F_{x,i}, \delta_{f,i}\right]^{\mathrm{T}}$ is the control input.

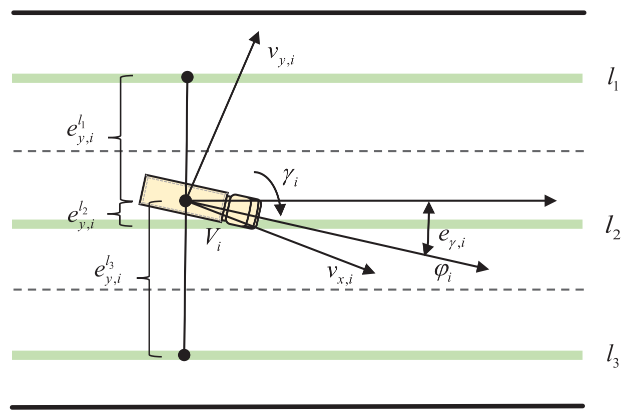

Fig. 2. Lateral vehicle kinematics.

The constraint of the control input $\hat{u}_i$ is

$$\hat{u}_i \in \hat{\mathcal{U}} := \left\{ \hat{u}_i \in \mathbb{R}^2 \,\middle|\, \begin{matrix} F_{x,i}^{min} \le F_{x,i} \le F_{x,i}^{max} \\ \delta_{f,i}^{min} \le \delta_{f,i} \le \delta_{f,i}^{max} \end{matrix} \right\}, \tag{7}$$

and the constraint of the state $\hat{x}_i$ is

$$\hat{x}_i \in \hat{\mathcal{X}} := \left\{ \hat{x}_i \in \mathbb{R}^3 \,\middle|\, \begin{matrix} v_{x,i}^{min} \le v_{x,i} \le v_{x,i}^{max} \\ v_{y,i}^{min} \le v_{y,i} \le v_{y,i}^{max} \\ \gamma_i^{min} \le \gamma_i \le \gamma_i^{max} \end{matrix} \right\}. \tag{8}$$

C. Inter-Vehicle Spacing Strategy

In general, either a constant inter-vehicle spacing policy or a constant time headway policy is adopted in vehicle platoons. The desired distance between vehicle i and its preceding vehicle j can be defined as

$$d_{des} = (i - j)d_0 \tag{9}$$

under the constant spacing policy, or as

$$d_{des} = T_h v_{x,i} + (i - j)d_0 \tag{10}$$

under the constant time headway policy. Here, d_0 is a predefined constant spacing, and T_h denotes the constant time headway.

D. Vehicle Kinematics

The lateral vehicle kinematics are shown in Fig. 2, where the road centerlines are denoted as l_1, l_2, and l_3, respectively.

The lateral displacement error between vehicle V_i and the centerline l_d is

$$e_{y,i}^{l_d} = p_{y,i} - p_y^{l_d}, \tag{11}$$

where $p_{y,i}$ is the lateral displacement of vehicle V_i, $p_y^{l_d}$ is the lateral position of the centerline l_d, $d \in \{1, 2, \ldots, nr\}$, and nr represents the number of centerlines.

Thus, lateral vehicle kinematics can be described as

$$\dot{e}_{y,i}^{l_d} = v_{x,i}e_{\varphi,i} - v_{y,i}, \tag{12a}$$

$$\dot{e}_{\varphi,i} = \dot{\varphi}_{i,des} - \dot{\varphi}_i, \tag{12b}$$

where $\varphi_{i,des}$ is the desired heading angle, and $\dot{\varphi}_i = \gamma_i$ is the yaw rate.

Then, (12) can be rewritten as

$$\dot{e}_{y,i}^{l_d} = v_{x,i} e_{\varphi,i} - v_{y,i}, \tag{13a}$$

$$\dot{e}_{\varphi,i} = \gamma_{i,des} - \gamma_i, \tag{13b}$$

where $\gamma_{i,des} = v_{x,i}/R$ is the desired yaw rate and R is the road radius. Note that $1/R = 0$ while the vehicle drives on a straight road.

The longitudinal displacement error between vehicle V_i and the desired preceding vehicle V_j is

$$e_{x,i} = p_{x,j} - p_{x,i} - (i - j)\, d_{des}. \tag{14}$$

Thus, by combining (13) and (14), the vehicle kinematic model is formulated as follows [47]:

$$\dot{e}_{x,i} = v_{x,j-1} - v_{x,i}, \tag{15a}$$

$$\dot{e}_{y,i}^{l_d} = v_{x,i} e_{\varphi,i} - v_{y,i}, \tag{15b}$$

$$\dot{e}_{\varphi,i} = \gamma_{i,des} - \gamma_i. \tag{15c}$$

Denote states and control inputs of the vehicle model (15) by $x_i = \left[e_{x,i}, e_{y,i}^{l_d}, e_{\varphi,i}\right]^{\mathrm{T}}$ and $u_i = \left[u_i^1, u_i^2, u_i^3\right]^{\mathrm{T}}$, respectively, where

$$\begin{cases} u_i^1 = v_{x,i-1} - v_{x,i} \\ u_i^2 = v_{y,i} \\ u_i^3 = \gamma_{i,des} - \gamma_i. \end{cases} \tag{16}$$

Then, a discrete linear parameter-varying (LPV) model is developed as

$$x_i(k+1) = A_i\left(v_{x,i}\right) x_i(k) + B_i u_i(k), \tag{17}$$

where

$$A_i\left(v_{x,i}\right) = \begin{bmatrix} 1 & 0 & 0 \\ 0 & 1 & \tau_1 v_{x,i} \\ 0 & 0 & 1 \end{bmatrix}, B_i = \begin{bmatrix} \tau_1 & 0 & 0 \\ 0 & -\tau_1 & 0 \\ 0 & 0 & \tau_1 \end{bmatrix}.$$

Note that A_i is with respect to $v_{x,i} \in \left[v_{x,i}^{min}, v_{x,i}^{max}\right]$ according to (8). Thus, $A_i\left(v_{x,i}\right)$ lies within a convex hull of matrices, i.e.,

$$A_i\left(v_{x,i}\right) \in \mathrm{Co}\left\{A_i^{min}, A_i^{max}\right\}, \tag{18}$$

where $\mathrm{Co}\{\cdot\}$ denotes a convex hull of matrices, A_i^{min} corresponds to $v_{x,i} = v_{x,i}^{min}$, and A_i^{max} corresponds to $v_{x,i} = v_{x,i}^{max}$. Note that the system (17) is controllable if the sampling time $\tau_1 > 0$.

Remark 1: Inter-vehicle spacing policies include the constant spacing, constant time headway, and variable time headway methods [48]. Determining the optimal inter-vehicle spacing policy is beyond the scope of this paper.

E. Hierarchical Control

As shown in Fig. 3, the hierarchical control scheme of vehicle platoons consists of the decision-making layer and the control layer. In the decision-making layer, an FSM is developed, including the vehicle-following, gap-generation, and lane-changing phases. It outputs the decisions on the desired preceding vehicle and centerline for each vehicle, that is, the communication matrix $\mathcal{A}$ of the vehicle platoon and the desired centerline d for each vehicle are defined in

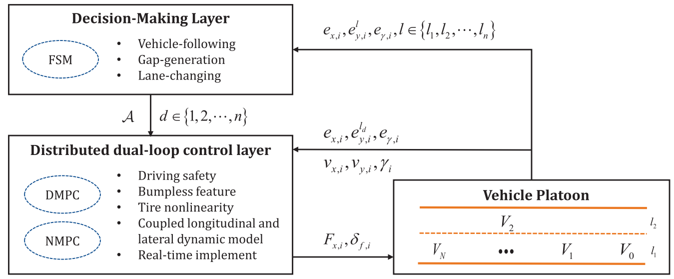

Fig. 3. Hierarchical control scheme for vehicle platoons.

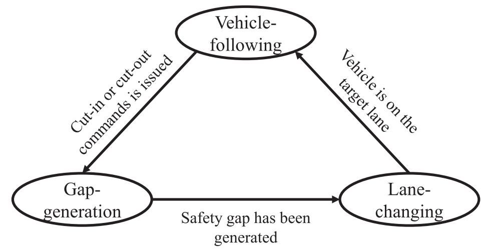

Fig. 4. Phase switching diagram of the FSM.

each phase, respectively. Then, in the control layer, DMPC and NMPC are designed to output the control signals $F_{x,i}$ and $\delta_{f,i}$, where the driving safety, bumpless feature, tire nonlinearity, coupled longitudinal and lateral dynamics, and real-time implementation are considered.

Remark 2: In this paper, the problem of only a single vehicle merging into or splitting from a platoon is considered. The case of multiple vehicles merging into or splitting from a vehicle platoon is beyond the scope of this paper.

III. Decision-Making Layer

The phase switching diagram of the FSM is shown in Fig. 4. Details of each phase are described as follows.

A. Phases of the FSM

1) Vehicle-Following Phase: At the initial time instant $k = 0$, the vehicle platoon is in the vehicle-following phase. The vehicles are denoted from V_0 to V_N such that the following inequality holds:

$$p_{x,i-1} \geq p_{x,i}, i \in \{1, \ldots, N\}. \tag{19}$$

In this phase, all vehicles are in the same lane. For the communication matrix $\mathcal{A}$, $a_{i,i-1} = 1$ for $i \in \{1, 2, \ldots, N\}$, and all other entries are zero. The desired centerlines of all vehicles are aligned with those of the leading vehicle V_0.

2) Gap-Generation Phase: This phase aims to generate a safety gap for cut-in or cut-out maneuvers. Once a safety gap is generated, the vehicle platoon switches to the lane-changing phase. Otherwise, the vehicle platoon remains in the gap-generation phase. The desired preceding vehicles are defined as follows:

- For the cut-in maneuver, the cut-in vehicle V_c does not send information to other vehicles. The lagging vehicle V_{c+1} follows the preceding vehicle V_{c-1} to create a gap

for the cut-in vehicle. In the communication matrix $\mathcal{A}$, $a_{i,i-1} = 1$ for $i \in \{1, 2, \ldots, N\} \setminus \{c\}$, $a_{c+1,c-1} = 1$, and all other entries are zero.
- For the cut-out maneuver, the communication matrix $\mathcal{A}$ remains unchanged, i.e., $a_{i,i-1} = 1$ for $i \in \{1, 2, \ldots, N\}$.

Note that the actual safety gap is the desired inter-vehicle spacing for the cut-in and cut-out maneuvers. The strategy is that a vehicle platoon with the desired inter-vehicle spacing has been formulated in the longitudinal direction prior to the lane-changing phase.

In this phase, the cut-in or cut-out vehicle remains in its initial lane, that is, the lane-changing has not yet been executed.

3) Lane-Changing Phase: This phase involves the cut-in vehicle merging into the platoon or the cut-out vehicle splitting from it. The desired preceding vehicle and the desired centerline are defined as follows:

- For the cut-in maneuvers, the communication matrix is updated as $a_{i,i-1} = 1$ for $i \in \{1, 2, \ldots, N\}$. The desired centerline of vehicle V_c is aligned with that of the vehicle platoon.
- For the cut-out maneuvers, the communication matrix remains unchanged, i.e., $a_{i,i-1} = 1$ for $i \in \{1, 2, \ldots, N\}$. The desired centerline of vehicle V_c is adjusted to the target lane.

Remark 3: Determining the optimal position and timing for executing cut-in or cut-out maneuvers is beyond the scope of this paper.

B. Phase Switching Conditions

The phase switching conditions are defined as follows.

1) From "Vehicle-Following" to "Gap-Generation": If a cut-in or cut-out command is issued to the vehicle platoon, the vehicle platoon switches to the gap-generation phase. Otherwise, the vehicle platoon remains in the vehicle-following phase.

2) From "Gap-Generation" to "Lane-Changing": The vehicle platoon switches to the lane-changing phase from the gap-generation phase if the state x_i satisfies the following constraints:

$$x_i \in \mathcal{C}_i := \left\{ x_i \in \mathbb{R}^3 \,\middle|\, \left|e_{x,i}\right| \le e_x^s, \left|e_{y,i}^{l_d}\right| \le e_y^s \right\}, \tag{20}$$

where both e_x^s and e_y^s are small positive constants. This indicates that the longitudinal and lateral control objectives have been accomplished if the tracking errors are sufficiently small.

3) From "Lane Changing" to "Vehicle-Following": If the cut-in or cut-out vehicle reaches the target lane, i.e., when the switching condition (20) is satisfied, the vehicle platoon switches to the vehicle-following phase.

IV. Control Layer

As shown in Fig. 5, the outer-loop controller is designed to generate the reference sequence ς_i, using the vehicle kinematics as the prediction model. The inner-loop controller is designed to generate the control signals $F_{x,i}$ and $\delta_{f,i}$ for each vehicle, based on the coupled longitudinal and lateral vehicle dynamics. Typically, both the prediction horizon and the sampling time of the outer-loop are larger than those of the inner-loop to ensure computational efficiency. Consequently, the prediction horizons satisfy $h \ge \tilde{h}$, and the sampling times satisfy $\tau_1 \ge \tau_2$.

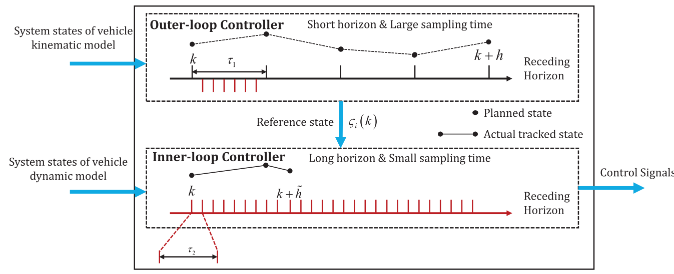

Fig. 5. Distributed dual-loop control layer.

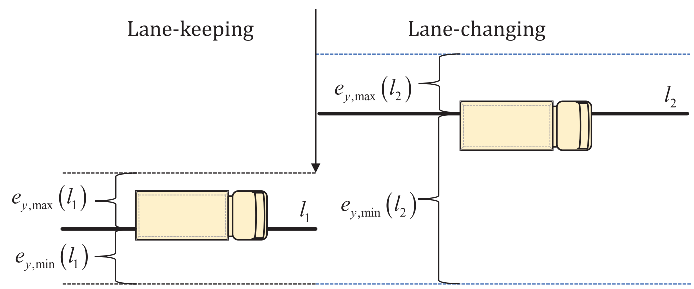

Fig. 6. Constraints of lateral displacement error.

A. Outer-Loop Controller

In this section, DMPC is designed to generate the desired longitudinal velocity, lateral velocity, and yaw rate in the outer-loop. To achieve asymptotic consensus of the vehicle platoon and ensure real-time implementation of the proposed DMPC, an efficient method is formulated.

1) Control Objective: The control objectives of vehicle V_i are to follow the desired preceding vehicle V_j and track the desired centerline l_d, that is,

$$\begin{cases} \lim\limits_{k\to\infty} e_{x,i}(k) = 0, \\ \lim\limits_{k\to\infty} e_{y,i}^{l_d}(k) = 0, \\ \lim\limits_{k\to\infty} e_{\varphi,i}(k) = 0, \end{cases} \tag{21}$$

where $i \in \{1, 2, \cdots, N\}$.

For the collision avoidance with the preceding vehicle, the longitudinal displacement error has

$$e_{x,i} \ge e_{x,i}^{min}, \tag{22}$$

where $e_{x,i}^{min} = d_{safe} - d_0$. Here, $d_{safe} = d_{brake} - (i - j)d_0$ represents the minimum safe inter-vehicle spacing, and d_{brake} is the braking distance.

While the gaps between the cut-in vehicle V_c and its preceding vehicle V_{c-1}, and between the cut-in vehicle V_c and its following vehicle V_{c+1} satisfy $x_i \in \mathcal{C}_i$, the vehicle platoon switches from the lane-changing phase to the vehicle-following phase. The longitudinal displacement error is smaller than $d_0 + 2e^s_x$. Thus, the maximum longitudinal displacement error is set to $e^{max}_{x,i} = d_0 + 2e^s_x$.

Furthermore, as shown in Fig. 6, the constraint on the lateral displacement error of the vehicle is defined with respect to the centerlines. Therefore, the constraint to prevent the lateral displacement error from exceeding the road boundaries is as follows:

$$e^{min}_{y,i}(l_d) \le e^{l_d}_{y,i}(k) \le e^{max}_{y,i}(l_d), \tag{23}$$

where $e^{min}_{y,i}(l_d)$ and $e^{max}_{y,i}(l_d)$ are the minimum and maximum lateral displacement errors with respect to the desired centerline l_d, respectively.

By (22) and (23), the state constraint set can be reformulated as

$$\mathcal{X}^{l_d}_i := \left\{x_i \in \mathbb{R}^3 \left| x^{min}_i(l_d) \le x_i \le x^{max}_i(l_d)\right.\right\}, \tag{24}$$

where

$$x^{min}_i(l_d) = \left[e^{min}_{x,i}, e^{min}_{y,i}(l_d), e^{min}_{\varphi,i}\right]^T$$

and

$$x^{max}_i(l_d) = \left[e^{max}_{x,i}, e^{max}_{y,i}(l_d), e^{max}_{\varphi,i}\right]^T.$$

Furthermore, the switching condition (20) should satisfy

$$\mathcal{C}_i \subseteq \mathcal{X}_i. \tag{25}$$

Considering the trackability of the reference sequence, the constraints on the control input are defined as

$$\mathcal{U}_i := \left\{u_i \in \mathbb{R}^3 \left| u^{min}_i \le u_i \le u^{max}_i\right.\right\}. \tag{26}$$

To guarantee smooth actions of vehicles, i.e., bumpless transfer control for phase switching, the admissible set of input increment $\Delta u_i(k)$ is defined as

$$\Delta\mathcal{U}_i := \left\{\Delta u_i \in \mathbb{R}^3 \left| \Delta u^{min}_i \le \Delta u_i \le \Delta u^{max}_i\right.\right\}. \tag{27}$$

Note that the admissible set of input increments can be selected based on the maximum and minimum values of the longitudinal acceleration, lateral acceleration, and jerk of vehicles.

2) Distributed Model Predictive Control: The optimization problem for vehicle V_i at time instant k can be expressed as follows:

Problem 1

$$\underset{u^*_i}{\text{minimize}}\; J_i(k) \tag{28}$$

$$\text{subject to: } x_i(0|k) = x_i(k), \tag{29a}$$
$$u_i(-1|k) = u_i(k-1), \tag{29b}$$
$$x_i(t+1|k) = A_i\left(v_{x,i}(k)\right)x_i(t|k) + B_i u_i(t|k), \tag{29c}$$
$$x_i(t+1|k) \in \mathcal{X}_i(k), \tag{29d}$$
$$u_i(t|k) \in \mathcal{U}_i, \tag{29e}$$
$$\Delta u_i(t|k) \in \Delta\mathcal{U}_i, t \in \mathbb{Z}^+_{[1,h-1]} \tag{29f}$$
$$\kappa_i x_i(h|k) - u_i(h-1|k) \in \Delta\mathcal{U}_i, \tag{29g}$$
$$x_i(h|k) \in \Omega_i, \tag{29h}$$

where the term J_i is the cost function, i.e.,

$$J_i(k) = \sum_{t=0}^{h-1} L\left(x_i(t|k), u_i(t|k)\right) + F\left(x_i(h|k)\right), \tag{30}$$

In (30), the term L is the stage cost function, i.e.,

$$L\left(x_i(k), u_i(k)\right) = \|x_i(k)\|^2_{Q_i} + \|u_i(k)\|^2_{R_i}. \tag{31}$$

In (30) and (31), both Q_i and R_i represent positive definite weight matrices, $F(x_i(h|k)) = \|x_i(h|k)\|_{P_i}$ is the terminal penalty function, P_i is the terminal penalty matrix, and Ω_i is a terminal positive invariant set.

Define the optimal solution of Problem 1 by

$$u^*_i(k) = \left\{u^*_i(0|k) \ldots u^*_i(h-1|k)\right\}. \tag{32}$$

Then, by (16), the reference sequence is derived as

$$\begin{aligned}\zeta_i(t|k) &= \left[v^r_x(t|k), v^r_y(t|k), \gamma^r(t|k)\right]^T \\ &= \begin{bmatrix} v_{x,i-1} \\ 0 \\ \gamma_{i,des}\end{bmatrix} + \begin{bmatrix} -1 & 0 & 0 \\ 0 & 1 & 0 \\ 0 & 0 & -1\end{bmatrix} u^*_i(t|k)\end{aligned} \tag{33}$$

where v^r_x, v^r_y, and γ^r are the reference longitudinal velocity, lateral velocity, and yaw rate, respectively. The term $u^*_i(t \mid k)$ is obtained using the linear interpolation method on (32).

Note that, due to the controllability of the pair $\left(A_i\left(v_{x,i}\right), B_i\right)$, there exists a terminal control law κ_i and a positive definite matrix P_i satisfying the following inequality [49]:

$$\begin{aligned}&\left(A_i\left(v_{x,i}\right) + B_i\kappa_i\right)^T P_i \left(A_i\left(v_{x,i}\right) + B_i\kappa_i\right) - P_i \\ &\le -Q_i - \kappa^T_i R_i \kappa_i.\end{aligned} \tag{34}$$

Remark 4: For other traffic scenarios, only the FSMs in the hierarchical control scheme need to be redesigned, which can provide the desired preceding vehicle and road centerline for each vehicle.

3) Terminal Ingredients: By solving the inequality (34), the terminal penalty matrix and the terminal control law can be obtained. Subsequently, using the Schur complement method, a linear matrix inequality-based optimization problem can be formulated as follows [18]:

Problem 2

$$\underset{Y_i, S_i}{\text{maximize}}\,(\det(Y_i))^{1/3} \tag{35}$$

$$\text{subject to: } \begin{bmatrix} Y_i & * & * & * \\ A^{min}_i Y_i + B_i S_i & Y_i & * & * \\ Y_i & 0 & Q^{-1}_i & * \\ S_i & 0 & 0 & R^{-1}_i \end{bmatrix} \ge 0, \tag{36a}$$

$$\begin{bmatrix} Y_i & * & * & * \\ A^{max}_i Y_i + B_i S_i & Y_i & * & * \\ Q^{\frac{1}{2}}_i Y_i & 0 & I & * \\ R^{\frac{1}{2}}_i S_i & 0 & 0 & I \end{bmatrix} \ge 0, \tag{36b}$$

where Y_i is a symmetric positive definite matrix. Thus, the terminal control gain is $\kappa_i = S_i Y^{-1}_i$, the terminal penalty matrix is $P_i = Y^{-1}_i$.

Remark 5: Problem 2 can be solved using the 'mincx' function from the MATLAB LMI Control Toolbox [50].

Then, the terminal positive invariant set Ω_i can be defined as

$$\Omega_i := \left\{ x_i \in \mathbb{R}^3 \left| \begin{array}{l} \sigma_j x_i + \eta_j \ge 0, \\ \sigma_j \in \mathbb{R}^{3\times 3}, \\ \eta_j \in \mathbb{R}^3, \\ j = 1, \ldots, v, \\ v \in \mathbb{Z}^+ \end{array}\right.\right\}, \tag{37}$$

which satisfies the following conditions:

(A1) $\Omega_i \in \mathcal{X}_i^{l_d}, (0,0) \in \mathcal{X}_i^{l_d}, d \in \{1, 2, \ldots, nr\}$;

(A2) $\kappa_i x_i \in \mathcal{U}_i$, for all $x_i(k) \in \Omega_i$;

(A3) $\kappa_i \left(x_i^1 - x_i^2\right) \in \Delta\mathcal{U}_i$, for all $x_i^1, x_i^2 \in \Omega_i$

(A4) $\left(A_i\left(v_{x,i}\right) + B_i\kappa_i\right) x_i \in \Omega_i$, for all $x_i(k) \in \Omega_i$.

Note that in Problem 1, all of the constraints are linear. Therefore, a standard quadratic programming problem is formulated as shown in Appendix A.

4) Analysis of Asymptotic Consensus of Vehicle Platoons: In the FSM, the cooperative process of the vehicle platoon includes three phases. Theorem 1 demonstrates the recursive feasibility of Problem 1 in each phase and proves that vehicle V_i can asymptotically follow its preceding vehicle and track the desired centerline based on terminal conditions. Subsequently, the asymptotic consensus of the vehicle platoon during the vehicle-following maneuver is established in Theorem 2.

Theorem 1: If Problem 1 is feasible at the time instant $k = k_0$, it is always feasible for $k \geq k_0$. The states of system (17) can converge to zero as $k \to \infty$, i.e., the vehicle V_i can asymptotically follow its preceding vehicle and track the desired centerline.

Proof 1: See Appendix B.

Theorem 2: Suppose that Problem 1 has feasible solutions at the initial time instant in the vehicle-following phase. Then, the vehicle platoon achieves asymptotic consensus.

Proof 2: See Appendix C.

Remark 6: In this paper, only the predecessor-following communication topology is considered. If vehicle V_i can receive predictive states from neighboring vehicles (denoted by Π_i), the proposed control scheme can also be extended to other communication topologies. In such case, the cost function is redefined in terms of neighboring vehicles, that is,

$$L(x_i(k), u_i(k)) = \|x_i(k)\|_{Q_i}^2 + \|u_i(k)\|_{R_i}^2 + \sum_{j\in\Pi_i} \left\|x_i(k) - x_j(k)\right\|_{F_i}^2. \tag{38}$$

Note that the asymptotic consensus and recursive feasibility always hold if the weighting matrices satisfy [18]

$$Q_i \geq \sum_{j\in\Pi_i} F_i.$$

B. Inner-Loop Controller

Taking into account the coupled longitudinal and lateral dynamics, tire nonlinearity, and actuator saturation constraints, NMPC is developed to track the reference sequence.

The control objective in the inner-loop is to find an admissible control input $\hat{u}_i$ such that [51]

$$\lim_{k\to\infty} \left\|\hat{x}_{e,i}(k)\right\| = 0, \tag{39}$$

where

$$\hat{x}_{e,i}(k) = \hat{x}_i(k) - \zeta_i(k). \tag{40}$$

Furthermore, dynamics of the error system (40) can be described as

$$\hat{x}_{e,i}(k+1) = g\left(\hat{x}_{e,i}(k), \hat{u}_{e,i}(k)\right), \tag{41}$$

where the function g is parameter-dependent on ζ_i, and the control input $\hat{u}_{e,i}$ is an implicit function of $\hat{u}_i$ and ζ_i.

Then, a stage cost function is defined as follows:

$$\hat{L}\left(\hat{x}_{e,i}(k), \hat{u}_{e,i}(k)\right) = \left\|\hat{x}_{e,i}(k)\right\|_{\Gamma_x}^2 + \left\|\hat{u}_{e,i}(k)\right\|_{\Gamma_u}^2, \tag{42}$$

where both Γ_x and Γ_u are weighting matrices.

To track the reference sequence, an optimization problem for vehicle V_i is formulated as follows: **Problem 3**

$$\underset{\hat{u}_i^*(k)}{minimize}\ \hat{J}(\hat{x}_i(k), \Delta\hat{u}_i(k)), \tag{43}$$

$$\text{subject to: } \hat{x}_i(t|k) = \hat{x}_i(k), \tag{44a}$$
$$\hat{x}_i(t+1|k) = f(\hat{x}_i(t|k), \hat{u}_i(t|k)), \tag{44b}$$
$$\hat{x}_i(t|k) \in \hat{\mathcal{X}}_i, \tag{44c}$$
$$\hat{u}_i(t|k) \in \hat{\mathcal{U}}_i, \tag{44d}$$
$$\hat{x}_{e,i}\left(\tilde{h}|k\right) \in \hat{\Omega}_i, \tag{44e}$$

where $\hat{\Omega}_i := \left\{\hat{x}_i \in \mathbb{R}^3 \left| \hat{x}_i^T \Gamma_{\tilde{h}} \hat{x}_i \leq 1\right.\right\}$ is a terminal positive invariant set, and Γ_h is the terminal penalty matrix. The term $\hat{J}$ is the cost function, i.e.,

$$\hat{J}(\hat{x}_i(k), \hat{u}_i(k)) = \sum_{t=0}^{\tilde{h}-1} \hat{L}\left(\hat{x}_{e,i}(t+1|k), \hat{u}_{e,i}(t+1|k)\right) + \left\|\hat{x}_{e,i}\left(\tilde{h}\middle|k\right)\right\|_{\Gamma_{\tilde{h}}}^2. \tag{45}$$

Define the optimal solution of Problem 3 by

$$\hat{u}_i^*(k) = \left\{\hat{u}_i^*(0|k) \ldots \hat{u}_i^*\left(\tilde{h}-1\middle|k\right)\right\}. \tag{46}$$

The first element $\hat{u}_i^*(0 \mid k)$ of the optimal solution (46) is sent to the vehicle at the time instant k. Then, Problem 3 is solved at the next time instant $k+1$, repeatedly.

Lemma 1 ([51], Theorem 1): Suppose that Problem 3 is feasible at the initial time, then,

(a) Problem 3 is always feasible for all time instants.

(b) The vehicle state $\hat{x}_i$ can track the reference sequence ζ_i, asymptotically.

1) Terminal Set and Penalty Matrix: To calculate the terminal ingredients, a method based on the PLDI is adopted [51].

Firstly, define the control input $\hat{u}_{e,i}$ as

$$\hat{u}_{e,i}(k) = \begin{bmatrix} \frac{F_{xr,i}(k)}{m} + \frac{\Delta v_{x,i}^r(k)}{\tau_2} + \gamma_i(k) v_{y,i}^r(k) \\ \frac{F_{yf,i}(k)+F_{yr,i}(k)}{m} + \frac{\Delta v_{y,i}^r(k)}{\tau_2} - \gamma_i(k) v_{x,i}^r(k) \\ \frac{l_f F_{yf,i}(k) - l_r F_{yr,i}(k)}{I_z} + \frac{\Delta \gamma_i^r(k)}{\tau_2} \end{bmatrix}. \tag{47}$$

Thus, there exists a set Σ_0 such that the following condition holds

$$g\left(\hat{x}_{e,i}, \hat{u}_{e,i}\right) \in \Sigma_0 \begin{bmatrix} \hat{x}_{e,i} \\ \hat{u}_{e,i} \end{bmatrix} \tag{48}$$

Considering that $\hat{\mathcal{X}}_i$ is compact, Σ_0 is bounded by a PLDI

$$\Sigma := \left\{\left[\hat{A}^{max}, \hat{B}\right], \left[\hat{A}^{min}, \hat{B}\right]\right\}, \tag{49}$$

where $\hat{B} = diag(\tau_2, \tau_2, \tau_2)$,

$$\hat{A}^{max} = \begin{bmatrix} 1 & \tau_2\gamma_i^{max}(k) & 0 \\ -\tau_2\gamma_i^{max}(k) & 1 & 0 \\ 0 & 0 & 1 \end{bmatrix}, \tag{50}$$

and

$$\hat{A}^{min} = \begin{bmatrix} 1 & \tau_2\gamma_i^{min}(k) & 0 \\ -\tau_2\gamma_i^{min}(k) & 1 & 0 \\ 0 & 0 & 1 \end{bmatrix}. \quad (51)$$

Lemma 2 ([51], Theorem 1): There have a matrix $\Upsilon \geq 0$ and a matrix $Z \in \mathbb{R}^{3\times3}$ such that, for all $\hat{A} \in \{\hat{A}^{\min}, \hat{A}^{\max}\}$, the following linear matrix inequalities hold:

$$\begin{bmatrix} \hat{A}\Upsilon + \hat{B}Z + (\hat{A}\Upsilon + \hat{B}Z)^T & * & * \\ \Upsilon & -\Gamma_x^{-1} & * \\ Z & 0 & -\Gamma_u^{-1} \end{bmatrix} \leq 0$$

Then, the terminal penalty matrix is $\Gamma_{\tilde{h}} = \Upsilon^{-1}$.

Algorithm 1 Hierarchical Control for the Vehicle Platoon

Offline:

Measure the state of each vehicle $\hat{x}_i(0)$. Set $\hat{x}_i(-1) = \hat{x}_i(0)$. Choose the weight matrices Q_i, R_i, Γ_x, and Γ_u. Choose the sampling times τ_1 and τ_2. Calculate the terminal ingredients by solving Problem 2. Define sets $k_{out} \triangleq \{\tau_1 k | k \in \mathbb{N}\}$ and $k_{in} \triangleq \{\tau_2 k | k \in \mathbb{N}\}$.

Online:

1) Set $k = 0$;
2) The decision-making layer determines the communication topology of vehicle platoons and the desired road center-lines for each vehicle;
3) Measure the states $x_i(k)$ and $\hat{x}_i(k)$ at time instant k;
4) Update the state constraint $\mathcal{X}_i(k)$;
5) if $k \in k_{out}$, obtain the reference sequence by solving Problem 1;
6) if $k \in k_{in}$, obtain the solution by solving Problem 3;
7) The first control input $\hat{u}_i^*(0|k)$ is applied to vehicle V_i;
8) Set $k = k + \tau_2$, and go to Step 2.

Problem 3 can be solved by an efficient Newton-type method with a look-up table in [52].

Remark 7: An integrated control method refers to designing a controller that considers both the kinematics and dynamics of vehicles simultaneously, which is computationally complex, difficult to ensure asymptotic consensus of vehicle platoons. Thus, the dual-loop controller is designed, with different prediction horizons and sampling times in the outer-loop and inner-loop, respectively.

Remark 8: NMPC is developed to track the reference sequences of the outer-loop. Tracking errors may occur due to vehicle uncertainties, such as parameter perturbation and disturbance. Note that the recursive feasibility and asymptotic consensus of the vehicle platoon hold due to the inherent robustness of the NMPC while small uncertainties occur.

Remark 9: The NMPC without terminal constraints can also achieve asymptotic convergence to the reference trajectory if a suitable prediction horizon is selected [53], [54]. In [52], the simulation results show that a longer prediction horizon should be considered for trucks to asymptotically track the reference trajectory, compared to an MPC with terminal ingredients. However, long prediction horizon may result in a larger computational burden.

Remark 10: The asymptotic consensus of a vehicle platoon can be achieved using distributed sliding-mode controller [10], distributed triple-step controller [11], or distributed backstepping controller [55]. In order to ensure the driving safety of trucks, the inherent physical limitations of trucks (e.g., steering system rate limits, engine/brake torque saturation) should be imposed as hard constraints within the control framework to guarantee that all generated commands are executable in general. However, the above approaches can not handle constraints effectively. Therefore, DMPC is adopted for vehicle platoons due to its ability to handle constraints explicitly. To achieve asymptotic consensus in the vehicle platoon, terminal equality constraints are typically imposed in the DMPC scheme; specifically, the terminal errors in inter-vehicle spacing and longitudinal velocity are required to be zero [4], [17]. Note that solving an optimization problem with terminal equality constraints is difficult in general. In this paper, a polyhedral terminal inequality constraint is imposed in the DMPC scheme, which guarantees asymptotic consensus for the vehicle platoon while reducing the conservatism of the optimization problem.

TABLE II
PARAMETERS OF THE TEST VEHICLE

Symbol	Value	Unit	Symbol	Value	Unit
m	1800	kg	l_f	2.5	m
l_r	1.5	m	I_z	130421.8	$\text{kg}\cdot\text{m}^2$
B_f	4.579	–	C_f	1.5237	–
D_f	43226	–	E_f	−3.6477	–
B_r	4.579	–	C_r	1.5237	–
D_r	100862	–	E_r	−3.6477	–

TABLE III
PARAMETERS OF THE HIERARCHICAL CONTROL SCHEME

Symbol	Value	Symbol	Value
e_x^s	0.5 m	e_y^s	0.05 m
τ_1	0.5 s	τ_2	0.05 s
h	14	$\tilde{h}$	5
$e_{x,i}^{max}$	20.1 m	$e_{x,i}^{min}$	5 m
$e_{y,i}^{max}$	$\{2, 4, 6\}$	$e_{y,i}^{min}$	$\{-2, -4, -6\}$
$e_{\varphi,i}^{max}$	0.5 rad	$e_{\varphi,i}^{min}$	−0.5 rad
u_i^{max}	$[25, 2, 0.5]^{\mathrm{T}}$	u_i^{min}	$[-25, -2, -0.5]^{\mathrm{T}}$
Δu_i^{max}	$[5, 1, 0.5]^{\mathrm{T}}$	Δu_i^{min}	$[-2.5, -1, -0.5]^{\mathrm{T}}$
v_x^{max}	35 m/s	v_x^{min}	10 m/s
v_y^{max}	2 m/s	v_y^{min}	−2 m/s
γ^{max}	0.5 rad/s	γ^{min}	−0.5 rad/s
F_x^{max}	105600 N	F_x^{min}	−211200 N
δ_f^{max}	0.7 rad	δ_f^{min}	−0.7 rad
Q_i	$diag(1, 15, 20)$	R_i	$diag(1, 2, 4)$
Γ_x	$diag(3 \times 10^5, 5 \times 10^7, 1.5 \times 10^6)$	Γ_u	$diag(1 \times 10^{-10}, 1 \times 10^{-2}, 1.1 \times 10^{-6})$

V. SIMULATION

To evaluate the performance of the proposed hierarchical control scheme, co-simulations are conducted using TruckSim and MATLAB/Simulink. A light-duty truck with four tires on the rear driving axle is used in the simulations, which has a larger mass compared to passenger vehicles. Note that the proposed scheme is not only effective for light-duty trucks but also for vehicles with similar dynamics, such as passenger cars and buses. The parameters of the vehicle are provided in

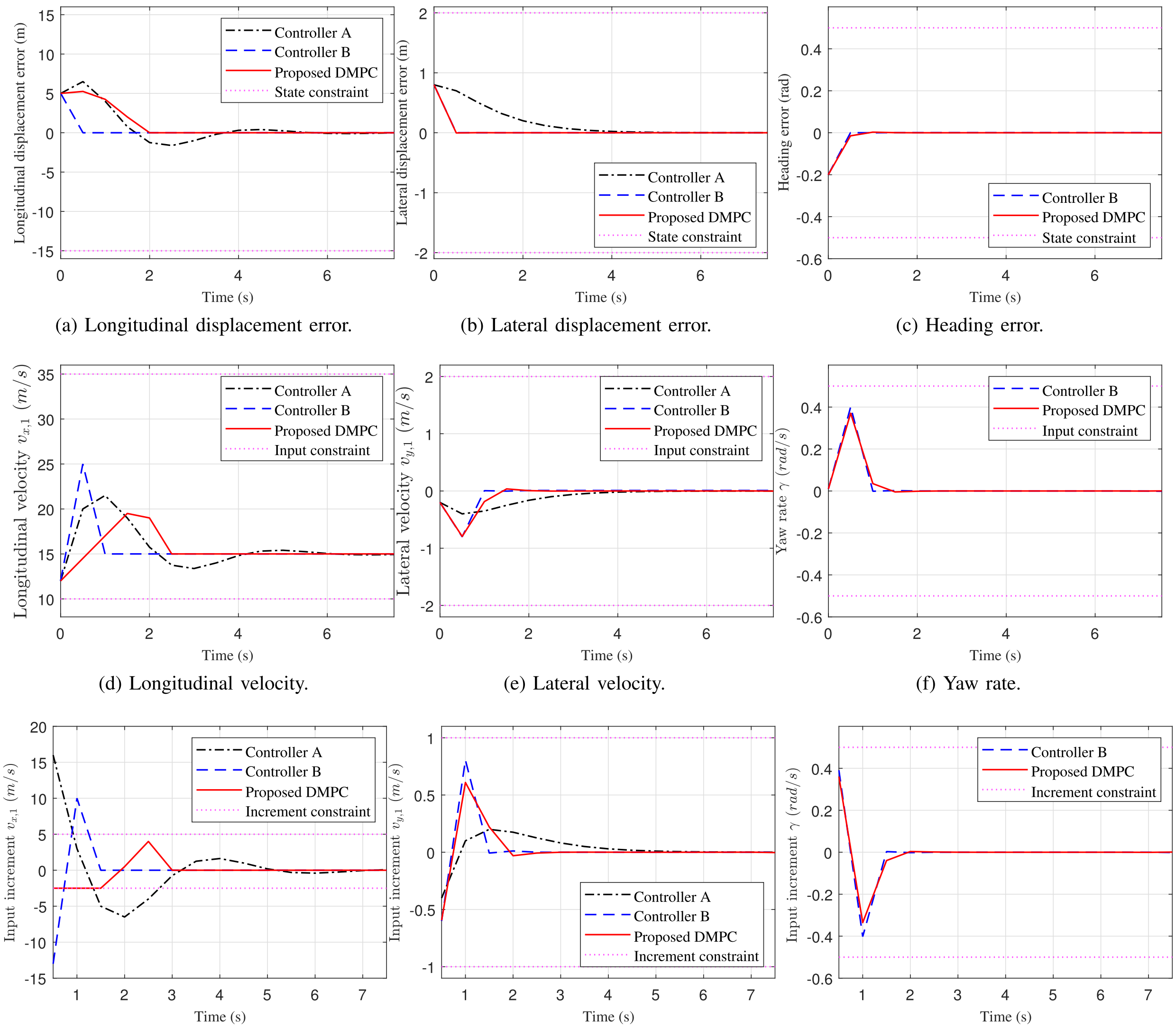

(a) Longitudinal displacement error. (b) Lateral displacement error. (c) Heading error.

(d) Longitudinal velocity. (e) Lateral velocity. (f) Yaw rate.

(g) Longitudinal velocity increment. (h) Lateral velocity increment. (i) Yaw rate increment.

Fig. 7. Reference sequence profiles of vehicle V_1 in Case 1.

Table II. Furthermore, the parameters of the decision-making layer and control layer are shown in Table III, respectively.

Then, the terminal penalty matrix P_i is

$$P_i = \begin{bmatrix} 16.847 & -3.045 & -25.530 \\ -3.045 & 67.143 & 192.074 \\ -25.530 & 192.074 & 1818.035 \end{bmatrix},$$

The terminal control gain K_i is

$$\kappa_i = \begin{bmatrix} -2.089 & 1.343 & 15.790 \\ 0.158 & 1.827 & 2.529 \\ -0.009 & -0.756 & -9.302 \end{bmatrix}.$$

The terminal penalty matrix $\Gamma_{\tilde{h}}$ is

$$\Gamma_{\tilde{h}} = \begin{bmatrix} 2.8292 \times 10^7 & * & * \\ 3.0803 \times 10^5 & 2.6477 \times 10^8 & * \\ -5.1186 \times 10^5 & 3.3141 \times 10^8 & 7.5004 \times 10^8 \end{bmatrix}. \quad (52)$$

A. *Tests for the Proposed Outer-Loop Controller*

To evaluate the performance of the DMPC in the outer-loop, two simulation scenarios are presented. The proposed DMPC considering constraints on states, inputs, and input increments is compared with a PID controller (Controller A) [29] and a DMPC without input increment constraints (Controller B) [18].

The simulation results are shown in Fig. 7 and Fig. 8, where the dash-dot black line, dashed blue line, and solid red line represent the reference sequence profiles of Controller A, Controller B, and the proposed DMPC, respectively. Note that the dash-dot horizontal lines indicate the maximum or minimum values. Furthermore, in Controller A, the yaw rate profiles are not considered.

Remark 11: For Controller A, a second-order kinematic model is adopted, which incorporates only the position and velocity of the vehicle. Therefore, the yaw rate response is excluded from the simulation results.

1) Case 1: The verification for the DMPC is implemented, where the vehicle platoon consists of two vehicles (a leading vehicle V_0 and a following vehicle V_1). The initial states of the leading vehicle are $v_{x,0}(0) = 15$m/s, $p_{x,0}(0) = 95$ m, $v_{y,0}(0) = 0$ m, $p_{y,0}(0) = 0$ m, $\varphi_0(0) = 0$ rad, and

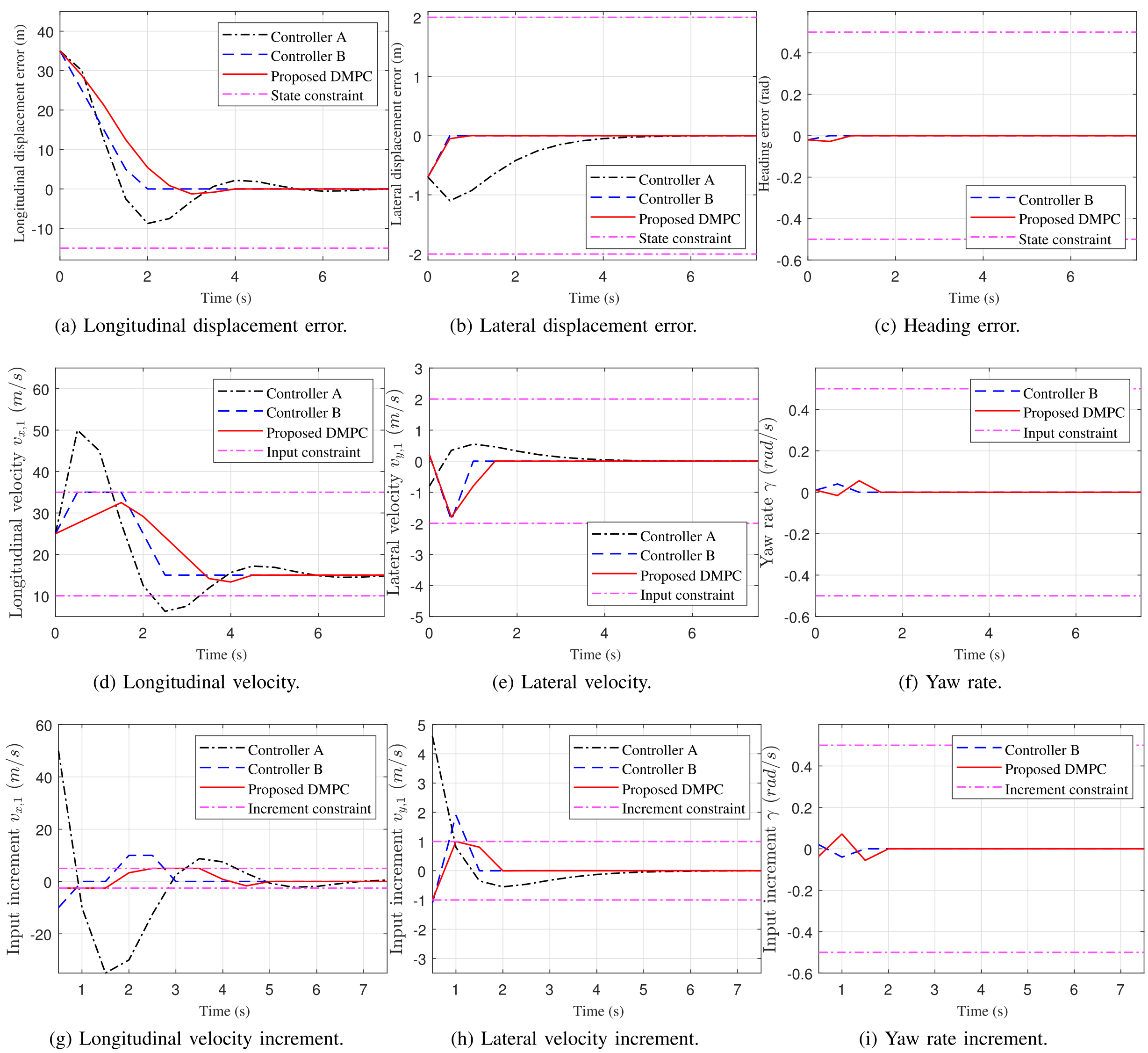

(a) Longitudinal displacement error. (b) Lateral displacement error. (c) Heading error.

(d) Longitudinal velocity. (e) Lateral velocity. (f) Yaw rate.

(g) Longitudinal velocity increment. (h) Lateral velocity increment. (i) Yaw rate increment.

Fig. 8. Reference sequence profiles of vehicle V_1 in Case 2.

$\gamma_0(0) = 0$rad/s, respectively. Furthermore, the initial states of the following vehicle are $v_{x,1}(0) = 12$m/s, $p_{x,1}(0) = 70$ m, $v_{y,1}(0) = -0.2$m/s, $p_{y,1}(0) = -0.8$ m, $\varphi_1(0) = 0.2$ rad, and $\gamma_1(0) = -0.01$rad/s, respectively. Thus, there are $x_1(0) = [5, 0.8, -0.2]^{\mathrm{T}}$ and $u_1(0) = [3, -0.2, 0.01]^{\mathrm{T}}$.

As shown in Fig. 7a, Fig. 7b, and Fig. 7c, the longitudinal displacement error, lateral displacement error, and heading error of vehicles for all controllers converge to zero. For the Controller B, it converges to zero rapidly, due to disregard the input increment constraint. For the Controller A, the vehicle states have not only the slowest convergence rate, but also violate the constraints, as shown in Fig. 7a, Fig. 7d, and Fig. 7g. However, the longitudinal velocity of vehicles for both the Controller A and Controller B violates incremental constraints, as shown in Fig. 7g. Therefore, the longitudinal velocity profiles are not smooth, i.e., the bumpless transfer control of phase switching of vehicles can not be guaranteed. In summary, the proposed DMPC is effective in the outer-loop, offering a feasible reference sequence for the inner-loop.

2) Case 2: In this case, a larger inter-vehicle space is adopted than that in Case 1. This results in a larger longitudinal velocity increment under the same prediction horizon. Thus, it can be verified whether the proposed controller can effectively ensure the incremental constraints. The initial states of the leading vehicle are $v_{x,0}(0) = 15$m/s, $p_{x,0}(0) = 95$ m, $v_{y,0}(0) = 0$m/s, $p_{y,0}(0) = 0$ m, $\varphi_0(0) = 0$ rad, and $\gamma_0(0) = 0$ rad/s, respectively. Furthermore, the initial states of the following vehicle are $v_{x,1}(0) = 25$ m/s, $p_{x,1}(0) = 40$ m, $v_{y,1}(0) = -0.8$ m/s, $p_{y,1}(0) = 0.7$ m, $\varphi_1(0) = 0.02$ rad, and $\gamma_1(0) = 0.02$ rad/s, respectively. Thus, there are $x_1(0) = [35, -0.7, -0.02]^{\mathrm{T}}$ and $u_1(0) = [-10, -0.8, -0.02]^{\mathrm{T}}$, respectively.

As shown in Fig. 8a, Fig. 8b, and Fig. 8c, the state x_1 of vehicle V_1 for all controllers converges to zero. In Fig. 8d, both the Controller B and the proposed DMPC satisfy the constraint of the longitudinal velocity of vehicles. However, for Controller A, the longitudinal velocity of the vehicle violates the constraints and exhibits oscillations. Furthermore, as

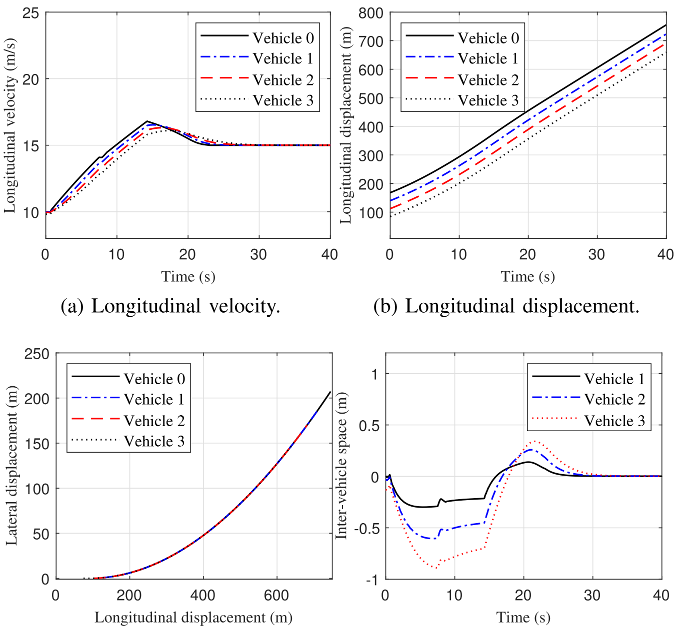

(a) Longitudinal velocity. (b) Longitudinal displacement.

(c) Lateral displacement. (d) Inter-vehicle spacing.

Fig. 9. Test results for the vehicle-following maneuver.

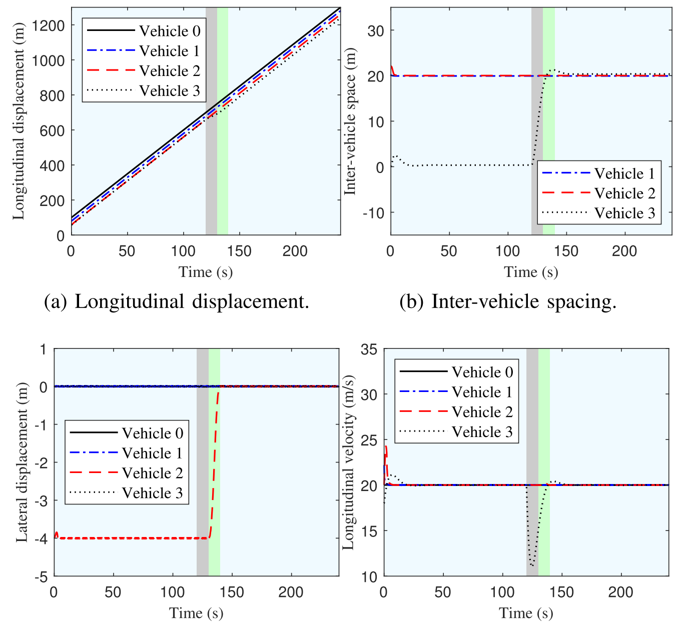

(a) Longitudinal displacement. (b) Inter-vehicle spacing.

(c) Lateral displacement. (d) Longitudinal velocity.

Fig. 10. Test results for the cut-in maneuver under a constant longitudinal velocity of the leading vehicle (The shaded regions denote different driving phases, i.e., vehicle-following phase; gap-generation phase; lane-changing phase).

shown in Fig. 8g, Fig. 8h, and Fig. 8i, for the proposed DMPC, the incremental constraints of the longitudinal velocity, lateral velocity, and yaw rate are satisfied. However, for both the Controller A and the Controller B, the incremental constraints cannot be guaranteed. Therefore, the bumpless transfer control of phase switching can be obtained, i.e., the vehicle has smooth actions.

In Figs. 7 and 8, the outer-loop controller provides reference sequences that satisfy the increment constraints. In comparison, the reference sequences of Controller A and Controller B, which do not take these constraints into account, may lead to handling instability in the vehicles. In summary, it is crucial to consider the incremental constraints.

B. Tests for the Proposed Hierarchical Control Scheme

A vehicle platoon consisting of four vehicles is used to demonstrate the proposed hierarchical control scheme for the vehicle-following, cut-in, and cut-out maneuver.

1) Tests for the Vehicle-Following Maneuver: The evaluation is conducted on a curved road. The leading vehicle V_0 follows a predefined acceleration profile, as illustrated in Fig. 9a. The time headway is set to $T_h = 0.8$. Set $d_0 = 20$ *m*. The simulation results under the predecessor-following communication topology are shown in Fig. 9. As shown in Fig. 9a, the longitudinal velocity responses of the following vehicles successfully track that of the leading vehicle. Fig. 9b presents the longitudinal displacement of each vehicle, indicating that no collisions occur within the platoon. Fig. 9c shows the lateral displacement of each vehicle, demonstrating that all vehicles can track the desired road centerline accurately. Moreover, Fig. 9d illustrates that the inter-vehicle spacing errors of the following vehicles converge to zero. It shows the effectiveness of the proposed hierarchical control scheme scheme.

2) Tests for the Cut-in Maneuver: Two experiments are conducted to evaluate the proposed scheme for the cut-in maneuver, specifically focusing on the constant longitudinal velocity and the time-varying longitudinal velocity of the leading vehicle.

Considering the scenario where the leading vehicle V_0 drives on a straight road at a constant velocity $v_{x,0} = 20$ m/s. The constant inter-vehicle spacing policy is adopted, where $d_0 = 20$ m. The simulation results are presented in Fig. 10. Note that the labels of all vehicles are not changed in order to clearly describe the process of the cut-in maneuver. The responses of inter-vehicle spacing can be deduced from the relative longitudinal displacements of the vehicles. At the initial time instant 0 s, the original vehicle platoon, consisting of vehicles V_0, V_1, and V_3, is in the vehicle-following phase. During the period from 0 s to 120 s, it maintains the desired inter-vehicle spacing without any collisions, as shown in Fig. 10a and Fig. 10b. At 120 s, the vehicle platoon switches to the gap-generation phase. Vehicle V_2 cuts into the platoon at 130 s as shown in Fig. 10c. At 140 s, a new vehicle platoon, consisting of vehicles V_0, V_1, V_2, and V_3, is formulated. The vehicle platoons always maintain a desired constant spacing. As shown in Fig. 10d, the longitudinal velocities of all vehicles satisfy the specified constraints.

Considering the scenario where the leading vehicle V_0 drives on a straight road at a time-varying longitudinal velocity. The constant time headway policy is adopted, where $d_0 = 10$ m and $T_h = 0.8$. The simulation results are presented in Fig. 11. At the initial time instant 0 s, the original vehicle platoon, consisting of vehicles V_0, V_1, and V_3, is in the vehicle-following phase. During the period from 0 s to 150 s, the platoon maintains the desired inter-vehicle spacing without any

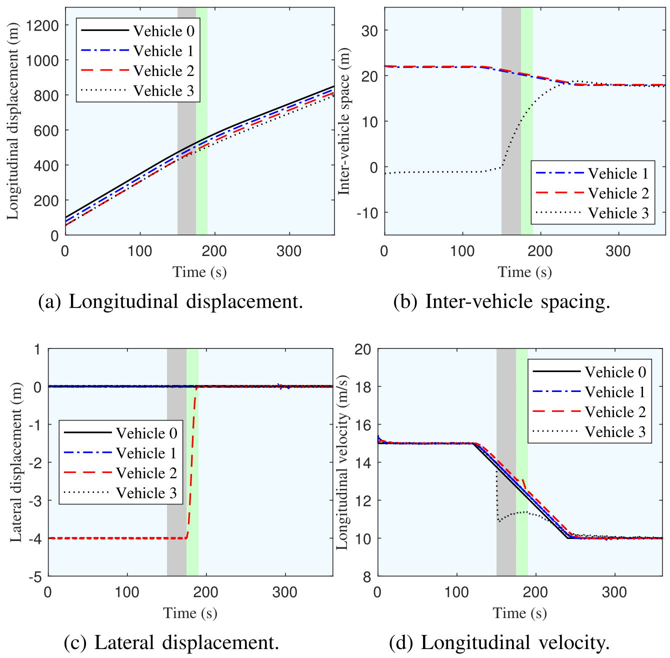

(a) Longitudinal displacement. (b) Inter-vehicle spacing.

(c) Lateral displacement. (d) Longitudinal velocity.

Fig. 11. Test results for the cut-in maneuver under time-varying longitudinal velocity of the leading vehicle (The shaded regions denote different driving phases, i.e., vehicle-following phase; gap-generation phase; lane-changing phase).

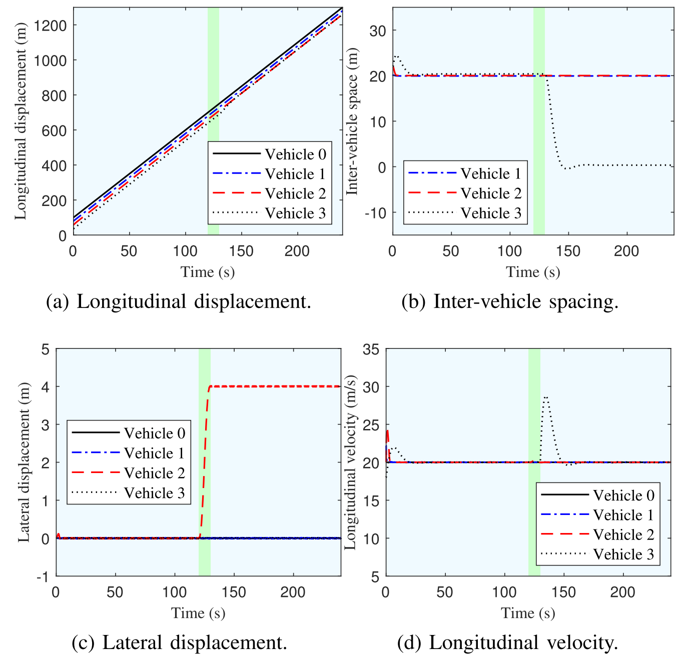

(a) Longitudinal displacement. (b) Inter-vehicle spacing.

(c) Lateral displacement. (d) Longitudinal velocity.

Fig. 12. Test results for the cut-out maneuver under a constant longitudinal velocity of the leading vehicle (The shaded regions denote different driving phases, i.e., vehicle-following phase; lane-changing phase).

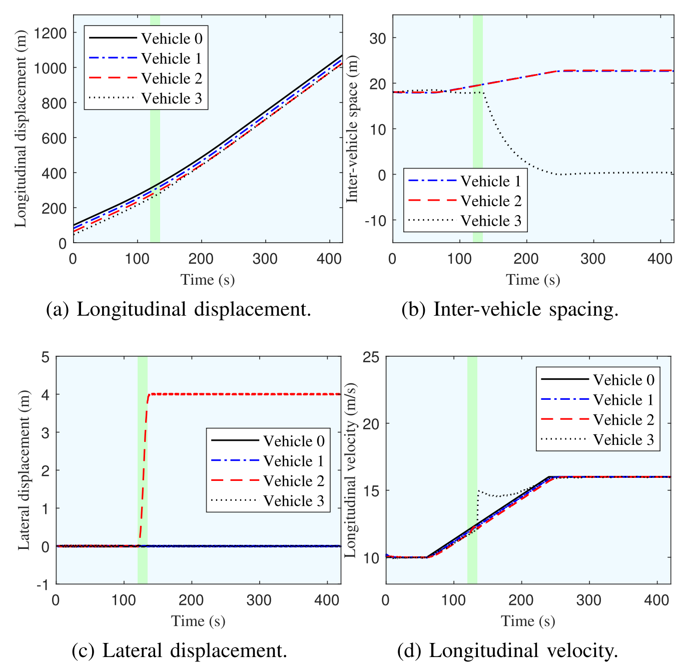

(a) Longitudinal displacement. (b) Inter-vehicle spacing.

(c) Lateral displacement. (d) Longitudinal velocity.

Fig. 13. Test results for the cut-out maneuver under time-varying longitudinal velocity of the leading vehicle (The shaded regions denote different driving phases, i.e., vehicle-following phase; lane-changing phase).

collisions, as shown in Fig. 11a and Fig. 11b. At 150 s, the vehicle platoon switches to the gap-generation phase. Vehicle V_2 cuts into the platoon at 175 s as shown in Fig. 11c. At 190 s, a new vehicle platoon, consisting of vehicles V_0, V_1, V_2, and V_3, is formulated. The vehicle platoons achieve the desired inter-vehicle spacing. As shown in Fig. 11d, the longitudinal velocities of all vehicles can track the longitudinal velocity of the leading vehicle.

3) Tests for the Cut-Out Maneuver: Two experiments are conducted to evaluate the proposed scheme for the cut-in maneuver, also specifically focusing on the constant longitudinal velocity and the time-varying longitudinal velocity of the leading vehicle.

Considering the scenario where the leading vehicle V_0 still drives on a straight road at a constant velocity $v_{x,0} = 20$ m/s. The constant inter-vehicle spacing policy is adopted, where $d_0 = 20$ m. The simulation results are presented in Fig. 12. The initial lateral displacement of the road centerline of the vehicle platoon is 0 m. At the initial time instant 0 s, the original platoon consisting of vehicles V_0, V_1, V_2, and V_3 is in the vehicle-following phase. As shown in Fig. 12a and Fig. 12b, during the period from 0 s to 120 s, the vehicle platoon maintains the desired constant spacing without any collisions. As shown in Fig 12c, vehicle V_2 leaves the platoon at 120 s. At 130 s, a new vehicle platoon consisting of vehicles V_0, V_1, and V_3 is formulated. In Fig. 12c, vehicle V_2 successfully tracks the desired road centerline. The vehicle platoons always maintain a desired constant spacing, as shown in Fig. 12b. The longitudinal velocities of all vehicles satisfy the specified constraints, as shown in Fig. 12d.

Considering the scenario where the leading vehicle V_0 still drives on a straight road at a time-varying longitudinal velocity. The constant time headway policy is adopted, where $d_0 = 10$ m and $T_h = 0.8$. The simulation results are presented in Fig. 13. The initial lateral displacement of the road centerline of the vehicle platoon is 0 m. At the initial time instant 0 s, the original platoon consisting of vehicles V_0, V_1, V_2, and V_3 is in the vehicle-following phase. As shown in Fig. 13a and Fig. 13b, during the period from 0 s to 120 s, the vehicle platoon maintains the desired inter-vehicle spacing

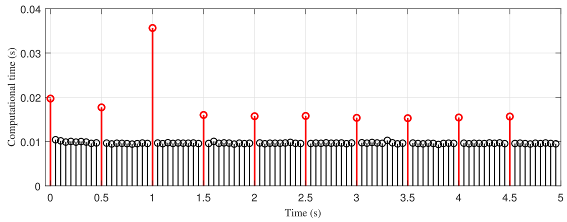

Fig. 14. Computation time of the proposed scheme for vehicle V_1.

without any collisions. As shown in Fig. 13c, vehicle V_2 leaves the platoon at 120 s. At 135 s, a new vehicle platoon consisting of vehicles V_0, V_1, and V_3 is formulated. In Fig. 13c, vehicle V_2 successfully tracks the desired road centerline. The vehicle platoons achieve the desired inter-vehicle spacing, as shown in Fig. 13b. The longitudinal velocities of all vehicles can track the longitudinal velocity of the leading vehicle, as shown in Fig. 13d.

C. Computational Time

The proposed hierarchical control scheme is implemented on a desktop computer equipped with a 2.90 GHz Intel(R) Core(TM) i7-10700 processor. In the outer-loop, Problem 1 is solved using the MATLAB function 'quadprog'. In the inner-loop, Problem 3 is solved using a Newton-type method based on a look-up table as described in [52].

Note that Problem 1 is essentially a quadratic programming problem, which can be solved efficiently with a computational complexity of $\mathcal{O}\left((h \times 3)^3\right)$. Considering the nonlinear tire model, a Newton-type method based on a look-up table is adopted to solve Problem 3, where the high computational complexity is reduced by online lookup of a precomputed hash-based tire table. The computational analysis of the Newton-type method based on a look-up table can be found in [52]. Moreover, the control frequence of vehicles should be higher than 10 Hz, i.e., the sampling time should be less than 0.1 s [56], [57]. In the outer loop, the sampling time is 0.5 s, while in the inner loop, it is 0.05 s.

The computation time of the proposed scheme is shown in Fig. 14. The red circles indicate the computation time at the sampling time $\tau_1 = 0.5$ s, while the black circles represent the computation time at the sampling time $\tau_2 = 0.05$ s. The maximum computation time is 0.0356 s, which is significantly shorter than the sampling time. Therefore, the proposed scheme is efficiently executable in real-time.

The simulations performed on a desktop computer naturally cannot fully represent real-world control performance. However, with the advancement of autonomous driving technologies, automotive-grade domain controller platforms, such as NVIDIA Jetson AGX Orin system on Module [58], Qualcomm Snapdragon Ride, and Huawei MDC [59], have been developed. These platforms offer computational capabilities surpassing those of typical desktop computers. Therefore, it is reasonable to assume that the proposed control strategy can be deployed for real vehicle control.

VI. Conclusion

In this paper, a hierarchical control scheme was proposed for the vehicle-following, cut-in, and cut-out maneuvers of vehicle platoons, consisting of the decision-making layer and the control layer. In the decision-making layer, an FSM was designed to divide the cooperative control process into the vehicle-following, gap-generation, and lane-changing phases with predefined switching conditions based on rules. In the control layer, DMPC based on the LPV vehicle kinematic model was proposed in the outer-loop, considering the collision avoidance and bumpless transfer control of vehicles. Furthermore, terminal ingredients of DMPC were calculated based on the linear matrix inequality. Then, the asymptotic consensus of the vehicle platoon was guaranteed. In the inner-loop, NMPC was designed considering the coupled longitudinal and lateral dynamics. For the real-time implementation of the proposed scheme, a standard quadratic programming problem for the outer-loop was formulated, and a Newton-type method was adopted for the inner-loop controller. The simulation results demonstrated the effectiveness of the proposed scheme.

Potential future research directions can be summarized as follows:

- Powertrain system control of autonomous trucks: This paper focuses on the control of truck longitudinal driving force and front-wheel steering angle, without incorporating the control of underlying engine or electric motor. It is challenging to design control schemes for the engine or electric motor to achieve energy savings in truck platooning systems, particularly due to the requirements for cooperative driving among multiple trucks.
- Decision-Making in complex transportation environments: 1) Developing control strategies for the dynamic merging and splitting of multi-platoons to enhance overall road capacity and adaptability on mixed-traffic highways; 2) Formulating macroscopic traffic models that incorporate multi-platoon behaviors to analyze their impact on traffic flow stability and efficiency.
- Fault-Tolerant control of vehicle platoons under cyber attacks: Developing distributed fault-tolerant control frameworks robust against cyber attacks targeting vehicular communication networks, such as delays, false data injection, and replay attacks.

Appendix A
Quadratic Programming Problem Formulation

Problem 1 can be transformed into a standard quadratic programming problem. First, define an input sequence as

$$U_i(k) \triangleq \begin{bmatrix} u_i(0\,|k) \\ u_i(1\,|k) \\ \vdots \\ u_i(h-1\,|k) \end{bmatrix}_{h\times 1}, \tag{53}$$

where the subscript symbol $h \times 1$ represents the quantities of vectors or submatrices within a matrix.

Then, a quadratic programming problem can be formulated as follows: **Problem 4**

$$\underset{U_i(k)}{\text{minimize}}\ U_i(k)^{\mathrm{T}}\Lambda_i U_i(k) - G_i(k)^{\mathrm{T}} U_i(k) \tag{54}$$

$$\text{subject to: } C_{ui} U_i(k) \geq B_{ui}(k), \tag{55}$$

where

$$\Lambda_i = S_{ui}^{\mathrm{T}}\Gamma_{xi}^{\mathrm{T}}\Gamma_{xi}S_{ui} + \Gamma_{ui}^{\mathrm{T}}\Gamma_{ui}, \tag{56}$$

$$G_i(k) = -2S_{ui}^{\mathrm{T}}\Gamma_{xi}^{\mathrm{T}}\Gamma_{xi}S_{xi}x_i(k), \tag{57}$$

$$C_{ui} = \begin{bmatrix} -W \\ W \\ -L \\ L \\ -S_{ui} \\ S_{ui} \\ D-\kappa_i DS_{ui} \\ \kappa_i DS_{ui}-D \\ \sigma_1 DS_{ui} \\ \vdots \\ \sigma_v DS_{ui} \end{bmatrix}_{(6h+2+v)\times 1}, \tag{58}$$

$$B_{ui}(k) = \begin{bmatrix} -u_i^{max} \\ \vdots \\ -u_i^{max} \\ u_i^{min} \\ \vdots \\ u_i^{min} \\ -\Delta u_i^{max} - u_i(k-1) \\ -\Delta u_i^{max} \\ \vdots \\ -\Delta u_i^{max} \\ \Delta u_i^{min} + u_i(k-1) \\ \Delta u_i^{min} \\ \vdots \\ \Delta u_i^{min} \\ S_{xi}x_i(k) - X_i^{max}(k) \\ -S_{xi}x_i(k) + X_i^{min}(k) \\ \kappa_i DS_{xi}x_i(k) - \Delta u_i^{max} \\ -\kappa_i DS_{xi}x_i(k) + \Delta u_i^{min} \\ -\eta_1 - \sigma_1 DS_{xi}x_i(k) \\ \vdots \\ -\eta_v - \sigma_v DS_{xi}x_i(k) \end{bmatrix}_{(6h+2+v)\times 1}, \tag{59}$$

$$S_{xi} = \begin{bmatrix} A_i \\ A_i^2 \\ \vdots \\ A_i^h \end{bmatrix}_{h\times 1}, \tag{60}$$

$$S_{ui} = \begin{bmatrix} B_i & 0 & \cdots & 0 \\ A_iB_i & B_i & \cdots & 0 \\ \vdots & \vdots & \ddots & \vdots \\ A_i^{h-1}B & A_i^{h-2}B_i & \cdots & B_i \end{bmatrix}_{h\times h}, \tag{61}$$

$$\Gamma_x \triangleq diag\{Q_i, Q_i, \ldots, P_i\}_{1\times h}, \tag{62}$$

$$\Gamma_u \triangleq diag\{R_i, R_i, \ldots, R_i\}_{1\times h}, \tag{63}$$

$$W = \begin{bmatrix} I_3 & 0 & 0 \\ \vdots & \ddots & \vdots \\ 0 & 0 & I_3 \end{bmatrix}_{h\times h}, \tag{64}$$

$$L = \begin{bmatrix} I_3 & 0 & \cdots & 0 \\ -I_3 & I_3 & \cdots & 0 \\ \vdots & \ddots & \ddots & \vdots \\ 0 & \cdots & -I_3 & I_3 \end{bmatrix}_{h\times h}, \tag{65}$$

$$X_i^{max}(k) = \begin{bmatrix} x_i^{max}(k) \\ \vdots \\ x_i^{max}(k) \end{bmatrix}_{h\times 1}, \tag{66}$$

$$X_i^{min}(k) = \begin{bmatrix} x_i^{min}(k) \\ \vdots \\ x_i^{min}(k) \end{bmatrix}_{h\times 1}, \tag{67}$$

and

$$D = [0, \cdots, I_3]_{1\times h}. \tag{68}$$

APPENDIX B
PROOF OF THEOREM 1

For different phases in the FSM, the recursive feasibility of Problem 1 and the vehicle V_i can follow the preceding vehicle and track the desired centerline asymptotically by the standard MPC arguments (see, e.g., [60]).

Namely, suppose that (32) is a feasible solution of Problem 1 at the time instant $k = k_0$. Then, at the next time instant $k+1$, a feasible solution can be selected as

$$u_i(k+1) = \begin{bmatrix} u_i^*(1|k) \\ \vdots \\ u_i^*(h-1|k) \\ \kappa_i x_i^*(h|k) \end{bmatrix}. \tag{69}$$

Thus, the recursive feasibility of Problem 1 is established. The optimal cost functional of the vehicle V_i is

$$J_i^*(k) = F\left(x_i^*(h|k)\right) + \sum_{t=0}^{h-1} L\left(x_i^*(t|k), u_i^*(t|k)\right). \tag{70}$$

Denote the cost function with (69) by

$$J_i(k+1) = F(x_i(h|k+1)) + \sum_{t=0}^{h-1} L(x_i(t|k+1), u_i(t|k+1)) \tag{71}$$

Thus,

$$\begin{aligned} &J_i(k+1) - J_i^*(k) \\ &= F(x_i(h|k)) \sum_{t=0}^{h-1} L(x_i(t|k), u_i(t|k)) - J_i^*(k) \\ &\le -L(x_i(0|k), u_i(0|k)) \\ &\quad + F(x_i(h|k+1)) - F(x_i(h|k)) \\ &= -\left\|x_i^*(0|k)\right\|_{Q_i} - \left\|u_i^*(0|k)\right\|_{R_i} \\ &\quad + F(x_i(h|k+1)) - F\left(x_i^*(h|k)\right), \end{aligned} \tag{72}$$

where

$$\begin{aligned} &F(x_i(h|k+1)) - F\left(x_i^*(h|k)\right) \\ &= \|x_i(h|k+1)\|_{P_i} - \left\|x_i^*(h|k)\right\|_{P_i} \\ &= \left\|\left(A_i\left(v_{x,i}(k)\right) + B_i\kappa_i\right)x_i^*(h|k)\right\|_{P_i} - \left\|x_i^*(h|k)\right\|_{P_i} \end{aligned}$$

$$\begin{aligned}&\leq -\left\| x_i^* \left(h \left| k \right. \right) \right\|_{Q_i+\kappa_i R_i \kappa_i}\\&\leq 0.\end{aligned} \tag{73}$$

Accordingly, it follows that:

$$J_i^* \left(k+1 \right) - J_i^* \left(k \right) \leq J_i \left(k+1 \right) - J_i^* \left(k \right) \tag{74}$$

In terms of (72) and (74), one has

$$J_i^* \left(k+1 \right) - J_i^* \left(k \right) \leq 0, \tag{75}$$

which indicates that the vehicle V_i can asymptotically follow its preceding vehicle and track the desired centerline.

Appendix C
Proof of Theorem 2

By the sum of the local cost function, a Lyapunov function of the vehicle platoon is defined as

$$\begin{aligned}J^* \left(k \right) &= \sum_{i=1}^{N} J_i^* \left(k \right)\\&= \sum_{i=1}^{N} \left\{ F\left(x_i^* \left(h \left| k \right. \right) \right) + \sum_{t=0}^{h-1} L\left(x_i^* \left(t \left| k \right. \right), u_i^* \left(t \left| k \right. \right) \right) \right\}.\end{aligned} \tag{76}$$

The sub-optimal cost function $J\left(k+1 \right)$ has:

$$J^* \left(k+1 \right) \leq J\left(k+1 \right). \tag{77}$$

Therefore,

$$J^* \left(k+1 \right) - J^* \left(k \right) \leq J\left(k+1 \right) - J^* \left(k \right). \tag{78}$$

Furthermore,

$$\begin{aligned}&J\left(k+1 \right) - J^* \left(k \right)\\&= \sum_{i=1}^{N} J_i \left(k+1 \right) - J^* \left(k \right)\\&= \sum_{i=1}^{N} \left\{ F\left(x_i \left(h \left| k \right. \right) \right) + \sum_{t=0}^{h-1} L\left(x_i \left(t \left| k \right. \right), u_i \left(t \left| k \right. \right) \right) \right\} - J^* \left(k \right)\\&\leq \sum_{i=1}^{N} \{ -L\left(x_i \left(0 \left| k \right. \right), u_i \left(0 \left| k \right. \right) \right)\\&\quad + F\left(x_i \left(h \left| k+1 \right. \right) \right) - F\left(x_i \left(h \left| k \right. \right) \right) \}\\&= \sum_{i=1}^{N} \left\{ -\left\| x_i^* \left(0 \left| k \right. \right) \right\|_{Q_i} - \left\| u_i^* \left(0 \left| k \right. \right) \right\|_{R_i} \right.\\&\quad \left. + F\left(x_i \left(h \left| k+1 \right. \right) \right) - F\left(x_i^* \left(h \left| k \right. \right) \right) \right\}.\end{aligned} \tag{79}$$

Then,

$$\begin{aligned}&J^* \left(k+1 \right) - J^* \left(k \right)\\&\leq -\sum_{i=1}^{N} \left\{ \left\| x_i^* \left(0 \left| k \right. \right) \right\|_{Q_i} + \left\| u_i^* \left(0 \left| k \right. \right) \right\|_{R_i} \right\}\\&\leq 0.\end{aligned} \tag{80}$$

Clearly, (80) shows that the cost function is strictly monotonically decreasing for the vehicle-following maneuver. Thus, the vehicle platoon achieves asymptotic consensus during the vehicle-following phase.

References

[1] A. L. Gratzer, S. Thormann, A. Schirrer, and S. Jakubek, "String stable and collision-safe model predictive platoon control," *IEEE Trans. Intell. Transp. Syst.*, vol. 23, no. 10, pp. 19358–19373, Oct. 2022.

[2] V. Turri, B. Besselink, and K. H. Johansson, "Cooperative look-ahead control for fuel-efficient and safe heavy-duty vehicle platooning," *IEEE Trans. Control Syst. Technol.*, vol. 25, no. 1, pp. 12–28, Jan. 2017.

[3] M. Martínez-Díaz, C. Al-Haddad, F. Soriguera, and C. Antoniou, "Impacts of platooning of connected automated vehicles on highways," *IEEE Trans. Intell. Transp. Syst.*, vol. 25, no. 7, pp. 6366–6396, Jul. 2024.

[4] Y. Zheng, S. E. Li, K. Li, F. Borrelli, and J. K. Hedrick, "Distributed model predictive control for heterogeneous vehicle platoons under unidirectional topologies," *IEEE Trans. Control Syst. Technol.*, vol. 25, no. 3, pp. 899–910, May 2017.

[5] M. R. Hidayatullah and J.-C. Juang, "Centralized and distributed control framework under homogeneous and heterogeneous platoon," *IEEE Access*, vol. 9, pp. 49629–49648, 2021.

[6] C. Desjardins and B. Chaib-Draa, "Cooperative adaptive cruise control: A reinforcement learning approach," *IEEE Trans. Intell. Transp. Syst.*, vol. 12, no. 4, pp. 1248–1260, Dec. 2011.

[7] H. Hao and P. Barooah, "Stability and robustness of large platoons of vehicles with double-integrator models and nearest neighbor interaction," *Int. J. Robust Nonlinear Control*, vol. 23, no. 18, pp. 2097–2122, Dec. 2013.

[8] Y. Zhu and F. Zhu, "Distributed adaptive longitudinal control for uncertain third-order vehicle platoon in a networked environment," *IEEE Trans. Veh. Technol.*, vol. 67, no. 10, pp. 9183–9197, Oct. 2018.

[9] Y. Li, C. Tang, K. Li, S. Peeta, X. He, and Y. Wang, "Nonlinear finite-time consensus-based connected vehicle platoon control under fixed and switching communication topologies," *Transp. Res. C, Emerg. Technol.*, vol. 93, pp. 525–543, Aug. 2018.

[10] Y. Zhu et al., "Finite-time cooperative control for vehicle platoon with sliding-mode controller and disturbance observer," *IEEE Trans. Intell. Transp. Syst.*, vol. 25, no. 9, pp. 10679–10688, Sep. 2024.

[11] H. Guo, J. Liu, Q. Dai, H. Chen, Y. Wang, and W. Zhao, "A distributed adaptive triple-step nonlinear control for a connected automated vehicle platoon with dynamic uncertainty," *IEEE Internet Things J.*, vol. 7, no. 5, pp. 3861–3871, May 2020.

[12] S. Shi, L. Li, Y. Mu, and G. Chen, "Stable headway prediction of vehicle platoon based on the 5-degree-of-freedom vehicle model," *Proc. Inst. Mech. Eng., D, J. Automobile Eng.*, vol. 233, no. 6, pp. 1570–1585, May 2019.

[13] P. Giselsson and A. Rantzer, "On feasibility, stability and performance in distributed model predictive control," *IEEE Trans. Autom. Control*, vol. 59, no. 4, pp. 1031–1036, Apr. 2014.

[14] S. Yu, M. Hirche, Y. Huang, H. Chen, and F. Allgöwer, "Model predictive control for autonomous ground vehicles: A review," *Auto. Intell. Syst.*, vol. 1, no. 1, pp. 1–17, Aug. 2021.

[15] W. B. Dunbar and D. S. Caveney, "Distributed receding horizon control of vehicle platoons: Stability and string stability," *IEEE Trans. Autom. Control*, vol. 57, no. 3, pp. 620–633, Mar. 2012.

[16] J. Zhan, Z. Ma, and L. Zhang, "Data-driven modeling and distributed predictive control of mixed vehicle platoons," *IEEE Trans. Intell. Vehicles*, vol. 8, no. 1, pp. 572–582, Jan. 2023.

[17] G. Nie, B. Xie, H. Lu, and Y. Tian, "A cooperative lane change approach for heterogeneous platoons under different communication topologies," *IET Intell. Transp. Syst.*, vol. 16, no. 1, pp. 53–70, Jan. 2022.

[18] Y. Feng et al., "Distributed MPC of vehicle platoons considering longitudinal and lateral coupling," *IEEE Trans. Intell. Transp. Syst.*, vol. 25, no. 3, pp. 2293–2310, Mar. 2024.

[19] F.-E. Braiteh, F. Bassi, and R. Khatoun, "Platooning in connected vehicles: A review of current solutions, standardization activities, cybersecurity, and research opportunities," *IEEE Trans. Intell. Vehicles*, vol. 10, no. 5, pp. 3134–3155, May 2025.

[20] Q. Li, Z. Chen, and X. Li, "A review of connected and automated vehicle platoon merging and splitting operations," *IEEE Trans. Intell. Transp. Syst.*, vol. 23, no. 12, pp. 22790–22806, Dec. 2022.

[21] I. A. Ntousakis, I. K. Nikolos, and M. Papageorgiou, "Optimal vehicle trajectory planning in the context of cooperative merging on highways," *Transp. Res. C, Emerg. Technol.*, vol. 71, pp. 464–488, Oct. 2016.

[22] Y. Lu, B. Wang, L. Huang, N. Zhao, and R. Su, "Modeling of driver cut-in behavior towards a platoon," *IEEE Trans. Intell. Transp. Syst.*, vol. 23, no. 12, pp. 24636–24648, Dec. 2022.

[23] S. Hwang, K. Lee, H. Jeon, and D. Kum, "Autonomous vehicle cut-in algorithm for lane-merging scenarios via policy-based reinforcement learning nested within finite-state machine," *IEEE Trans. Intell. Transp. Syst.*, vol. 23, no. 10, pp. 17594–17606, Oct. 2022.

[24] D. Liu, S. Mair, K. Yang, S. Baldi, P. Frasca, and M. Althoff, "Resilience in platoons of cooperative heterogeneous vehicles: Self-organization strategies and provably-correct design," *IEEE Trans. Intell. Vehicles*, vol. 9, no. 1, pp. 2262–2275, Jan. 2024.

[25] P. Liu, A. Kurt, and U. Ozguner, "Distributed model predictive control for cooperative and flexible vehicle platooning," *IEEE Trans. Control Syst. Technol.*, vol. 27, no. 3, pp. 1115–1128, May 2019.

[26] M. H. Basiri, B. Ghojogh, N. L. Azad, S. Fischmeister, F. Karray, and M. Crowley, "Distributed nonlinear model predictive control and metric learning for heterogeneous vehicle platooning with cut-in/cut-out maneuvers," in *Proc. 59th IEEE Conf. Decis. Control (CDC)*, Dec. 2020, pp. 2849–2856.

[27] W. J. Scholte, P. W. A. Zegelaar, and H. Nijmeijer, "A control strategy for merging a single vehicle into a platoon at highway on-ramps," *Transp. Res. C, Emerg. Technol.*, vol. 136, Mar. 2022, Art. no. 103511.

[28] J. Wu, Y. Wang, and C. Yin, "Curvilinear multilane merging and platooning with bounded control in curved road coordinates," *IEEE Trans. Veh. Technol.*, vol. 71, no. 2, pp. 1237–1252, Feb. 2022.

[29] J. Wu, Y. Wang, Z. Shen, L. Wang, H. Du, and C. Yin, "Distributed multilane merging for connected autonomous vehicle platooning," *Sci. China Inf. Sci.*, vol. 64, no. 11, Nov. 2021, Art. no. 212202.

[30] A. Irshayyid and J. Chen, "Comparative study of cooperative platoon merging control based on reinforcement learning," *Sensors*, vol. 23, no. 2, p. 990, Jan. 2023.

[31] M. Li, Z. Li, B. Wang, and S. Wang, "A bounded rationality-aware car-following strategy for alleviating cut-in events and traffic disturbances in traffic oscillations," *IEEE Trans. Intell. Transp. Syst.*, vol. 25, no. 11, pp. 17902–17916, Nov. 2024.

[32] G. Du, Y. Zou, X. Zhang, J. Fan, W. Sun, and Z. Li, "Efficient motion control for heterogeneous autonomous vehicle platoon using multilayer predictive control framework," *IEEE Internet Things J.*, vol. 11, no. 23, pp. 38273–38290, Dec. 2024.

[33] X. Yang, H. Liu, M. Xu, and J. Wan, "Cooperative merging control based on reinforcement learning with dynamic waypoint," *IEEE Access*, vol. 12, pp. 81581–81592, 2024.

[34] Z. Wang, D. Sun, L. Wang, and M. Zhao, "Mixed vehicle group merging control in the vicinity of traffic signals: A cyber-physical perspective," *IEEE Trans. Intell. Transp. Syst.*, vol. 25, no. 6, pp. 5328–5341, Jun. 2024.

[35] W. Yang, Y. Chen, and Y. Su, "Enhancing connected autonomous vehicle formations: Discrete–offline–online three-layer architecture for platoon reconfiguration," *Int. J. Automot. Technol.*, vol. 25, no. 4, pp. 945–963, Aug. 2024.

[36] J. Wang et al., "Optimization design of the decentralized multi-vehicle cooperative controller for freeway ramp entrance," *Int. J. Automot. Technol.*, vol. 22, no. 3, pp. 799–810, Jun. 2021.

[37] S. Jing, F. Hui, X. Zhao, J. Rios-Torres, and A. J. Khattak, "Cooperative game approach to optimal merging sequence and on-ramp merging control of connected and automated vehicles," *IEEE Trans. Intell. Transp. Syst.*, vol. 20, no. 11, pp. 4234–4244, Nov. 2019.

[38] X. Duan, C. Sun, D. Tian, J. Zhou, and D. Cao, "Cooperative lane-change motion planning for connected and automated vehicle platoons in multi-lane scenarios," *IEEE Trans. Intell. Transp. Syst.*, vol. 24, no. 7, pp. 7073–7091, Jul. 2023.

[39] Y. Lu, L. Huang, J. Yao, and R. Su, "Intention prediction-based control for vehicle platoon to handle driver cut-in," *IEEE Trans. Intell. Transp. Syst.*, vol. 24, no. 5, pp. 5489–5501, May 2023.

[40] M. Amoozadeh, H. Deng, C.-N. Chuah, H. M. Zhang, and D. Ghosal, "Platoon management with cooperative adaptive cruise control enabled by VANET," *Veh. Commun.*, vol. 2, no. 2, pp. 110–123, Apr. 2015.

[41] C. Liu, Y. Luo, P. Li, C. Xing, and W. Kong, "An extendable maneuver management framework with fault-tolerant mechanism for vehicle platoon control system in highway scenario," *IET Intell. Transp. Syst.*, vol. 17, no. 10, pp. 2075–2088, Oct. 2023.

[42] H. Kim and F. Borrelli, "Facilitating cooperative and distributed multi-vehicle lane change maneuvers," *IFAC-PapersOnLine*, vol. 56, no. 2, pp. 5585–5590, 2023.

[43] J. Ivanchev, C. Deboeser, T. Braud, A. Knoll, D. Eckhoff, and A. Sangiovanni-Vincentelli, "A hierarchical state-machine-based framework for platoon manoeuvre descriptions," *IEEE Access*, vol. 9, pp. 128393–128406, 2021.

[44] Y. Ma, Z. Li, R. Malekian, S. Zheng, and M. A. Sotelo, "A novel multimode hybrid control method for cooperative driving of an automated vehicle platoon," *IEEE Internet Things J.*, vol. 8, no. 7, pp. 5822–5838, Apr. 2021.

[45] H. Zhang, L. Du, and J. Shen, "Hybrid MPC system for platoon based cooperative lane change control using machine learning aided distributed optimization," *Transp. Res. B, Methodol.*, vol. 159, pp. 104–142, May 2022.

[46] H. D. Nguyen, D. Kim, Y. S. Son, and K. Han, "Linear time-varying MPC-based autonomous emergency steering control for collision avoidance," *IEEE Trans. Veh. Technol.*, vol. 72, no. 10, pp. 12713–12727, Oct. 2023.

[47] C. Hu, R. Wang, F. Yan, and N. Chen, "Output constraint control on path following of four-wheel independently actuated autonomous ground vehicles," *IEEE Trans. Veh. Technol.*, vol. 65, no. 6, pp. 4033–4043, Jun. 2016.

[48] J. Chen, H. Liang, J. Li, and Z. Lv, "Connected automated vehicle platoon control with input saturation and variable time headway strategy," *IEEE Trans. Intell. Transp. Syst.*, vol. 22, no. 8, pp. 4929–4940, Aug. 2021.

[49] S. Yu et al., "Computation of terminal set for nonlinear model predictive control," *Acta Autom. Sinica*, vol. 48, no. 1, pp. 144–151, 2022.

[50] A. Nemirovskii and P. Gahinet, "The projective method for solving linear matrix inequalities," in *Proc. Amer. Control Conf.*, 1994, pp. 840–844.

[51] S. Yu, X. Li, H. Chen, and F. Allgöwer, "Nonlinear model predictive control for path following problems," *Int. J. Robust Nonlinear Control*, vol. 25, no. 8, pp. 1168–1182, May 2015.

[52] W. Li et al., "Nonlinear model predictive control of trajectory tracking for autonomous trucks with terminal ingredients," *Nonlinear Dyn.*, vol. 113, pp. 21383–21402, Jan. 2025.

[53] K. Berntorp, R. Quirynen, T. Uno, and S. Di Cairano, "Trajectory tracking for autonomous vehicles on varying road surfaces by friction-adaptive nonlinear model predictive control," *Vehicle Syst. Dyn.*, vol. 58, no. 5, pp. 705–725, May 2020.

[54] L. Grüne, "NMPC without terminal constraints," *IFAC Proc. Volumes*, vol. 45, no. 17, pp. 1–13, 2012.

[55] Z. Lv, J. Chen, J. Xie, and Z. Xu, "A backstepping tracking control strategy based on deep reinforcement learning for vehicle platoon," *IEEE Trans. Veh. Technol.*, vol. 74, no. 6, pp. 8707–8720, Jun. 2025.

[56] Intelligent Transport Systems—Cooperative Adaptive Cruise Control Systems (CACC)—Performance Requirements and Test Procedures, Standard ISO 20035:2019, Geneva, Switzerland, 2019.

[57] Intelligent Transport Systems—Truck Platooning Systems (TPS)—Functional and Operational Requirements, Standard ISO 4272:2022, Geneva, Switzerland, 2022.

[58] S. Sivashangaran and A. Eskandarian, "XTENTH-CAR: A proportionally scaled experimental vehicle platform for connected autonomy and all-terrain research," *ASME Int. Mech. Eng. Congr. Expo.*, vol. 87639, Jan. 2023, Art. no. V006T07A068.

[59] L. Chen et al., "Milestones in autonomous driving and intelligent vehicles—Part I: Control, computing system design, communication, HD map, testing, and human behaviors," *IEEE Trans. Syst., Man, Cybern., Syst.*, vol. 53, no. 9, pp. 5831–5847, Sep. 2023.

[60] S. Yu, T. Qu, F. Xu, H. Chen, and Y. Hu, "Stability of finite horizon model predictive control with incremental input constraints," *Automatica*, vol. 79, pp. 265–272, May 2017.

Wenbo Li received the B.S. and Ph.D. degrees in control science and engineering from Jilin University, China, in 2019 and 2025, respectively. His research interests include model predictive control, connected and automated vehicles, and vehicle stability control.

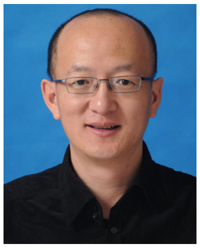

Shuyou Yu (Member, IEEE) received the B.S. and M.S. degrees in control science and engineering from Jilin University, China, in 1997 and 2005, respectively, and the Ph.D. degree in engineering cybernetics from the University of Stuttgart, Germany, in 2011. From 2010 to 2011, he was a Research and Teaching Assistant with the Institute for Systems Theory and Automatic Control, University of Stuttgart. In 2012, he joined as a Faculty Member with the Department of Control Science and Engineering, Jilin University, where he is currently a Full Professor. His main research interests include model predictive control, robust control, and its applications in mechatronic systems.

Yangyang Feng received the M.S. and Ph.D. degrees in control science and engineering from Jilin University, China, in 2019 and 2024, respectively. His research interests include distributed model predictive control and vehicle platoon control.

Haoran Qi received the B.S. degree in automation from Changchun University of Technology, China, in 2022, and the M.S. degree in control science and engineering from Jilin University, China, in 2025. His research interests include model predictive control and field-programmable gate arrays.

Hong Chen (Fellow, IEEE) received the B.S. and M.S. degrees in process control from Zhejiang University, China, in 1983 and 1986, respectively, and the Ph.D. degree in system dynamics and control engineering from the University of Stuttgart, Germany, in 1997. In 1986, she joined Jilin University of Technology, China. From 1993 to 1997, she was a Wissenschaftlicher Mitarbeiter with the Institut für Systemdynamik und Regelungstechnik, University of Stuttgart. Since 1999, she has been a Professor with Jilin University and hereafter a Tang Aoqing Professor. From 2015 to 2019, she was the Director of the State Key Laboratory of Automotive Simulation and Control. In 2019, she joined as a Distinguished Professor with Tongji University. Her current research interests include model predictive control, nonlinear control, and applications in mechatronic systems focusing on automotive systems.